2

DOE/MC/26050--3037

DE92 001110

Validation Testing of the EERC Pilot-Scale Circulating Fluidized-Bed Combustor Using Salt Creek Coal

Final Report

M.D. Mann
D.R. Hajicek
T.A. Moe
A.K. Henderson

September 1991

Work Performed Under Contract No.: DE-FG21-89MC26050

For
U.S. Department of Energy
Office of Fossil Energy
Morgantown Energy Technology Center
Morgantown, West Virginia

By
University of North Dakota
Energy and Environmental Research Center
Grand Forks, North Dakota

DISCLAIMER

DOE/MC/26050-3037
(DE92001110)

Validation Testing of the EERC Pilot-Scale Circulating Fluidized-Bed Combustor Using Salt Creek Coal

Final Report

M.D. Mann
D.R. Hajicek
T.A. Moe
A.K. Henderson

Work Performed Under Contract No.: DE-FG21-89MC26050

For
U.S. Department of Energy
Office of Fossil Energy
Morgantown Energy Technology Center
P.O. Box 880
Morgantown, West Virginia 26507-0880

By
University of North Dakota
Energy and Environmental Research Center
Box 8213
University Station
Grand Forks, North Dakota 58202

September 1991

TABLE OF CONTENTS

LIST OF FIGURES

LIST OF FIGURES (continued)

LIST OF TABLES

VALIDATION TESTING OF THE EERC PILOT-SCALE CIRCULATING FLUIDIZED-BED COMBUSTOR USING SALT CREEK COAL

1.0 INTRODUCTION

Project CFB was initiated in May 1988 under funding provided from the U.S. Department of Energy (DOE), the Empire State Electric Energy Research Corporation (ESEERCO), Northern States Power Company (NSP), the Electric Power Research Institute (EPRI), Otter Tail Power Company, North Dakota Lignite Research Council, ARCO Coal Company, TU Electric, Consolidated Edison of New York, Premier Refractories and Chemicals, and the University of North Dakota Energy and Environmental Research Center (EERC). The overall goal of the project was to provide a technical basis for assessing the economic and environmental feasibility of circulating fluidized-bed combustion (CFBC) technology, focusing on the effect of system configuration and coal properties on performance. Other underlying goals of the program were to 1) design and construct a CFBC test facility, thereby providing a test facility at an independent laboratory; 2) demonstrate that the test unit is capable of meeting the original design objectives; and 3) assess the ability of the unit to provide scalable data. The purpose of this interim report is to present data from validation testing to establish the scalability of data generated from this unit.

The 110-MW CFBC at the Colorado Ute Nucla Station has been successfully operating for the last several years. As it is one of EPRI's demonstration plants, EPRI was able to assemble a large data base characterizing the performance of this unit. In addition, EPRI and Pyropower participated in pilot plant testing in a pilot-scale CFBC in San Diego, CA. EERC obtained samples of the same coal and limestone used by those organizations and has operated its CFBC under similar operating conditions. This has provided the opportunity to compare the performance of the EERC CFBC with both a utility-scale plant and a vendor-operated pilot plant. Based on this comparison and supported by the information presented in this report, EERC feels confident that the 1-MW_{th} pilot-scale CFBC not only meets the original design objectives of Project CFB, but it also provides data that is scalable to a full-scale unit.

2.0 DESCRIPTION OF TEST FACILITIES

2.1 1-MW_{th} CFBC Test Facility

A schematic of the overall circulating fluidized-bed combustion system is shown in Figure 1. The overall system is divided up into the following systems:

- Combustion Air System,
- Flue Gas System,
- Flue Gas Recirculation System,
- Ash-Fouling Section,
- Coal and Sorbent System,
- Combustor,
- Solids Recirculation System,
- Natural Gas-Fired Preheater,

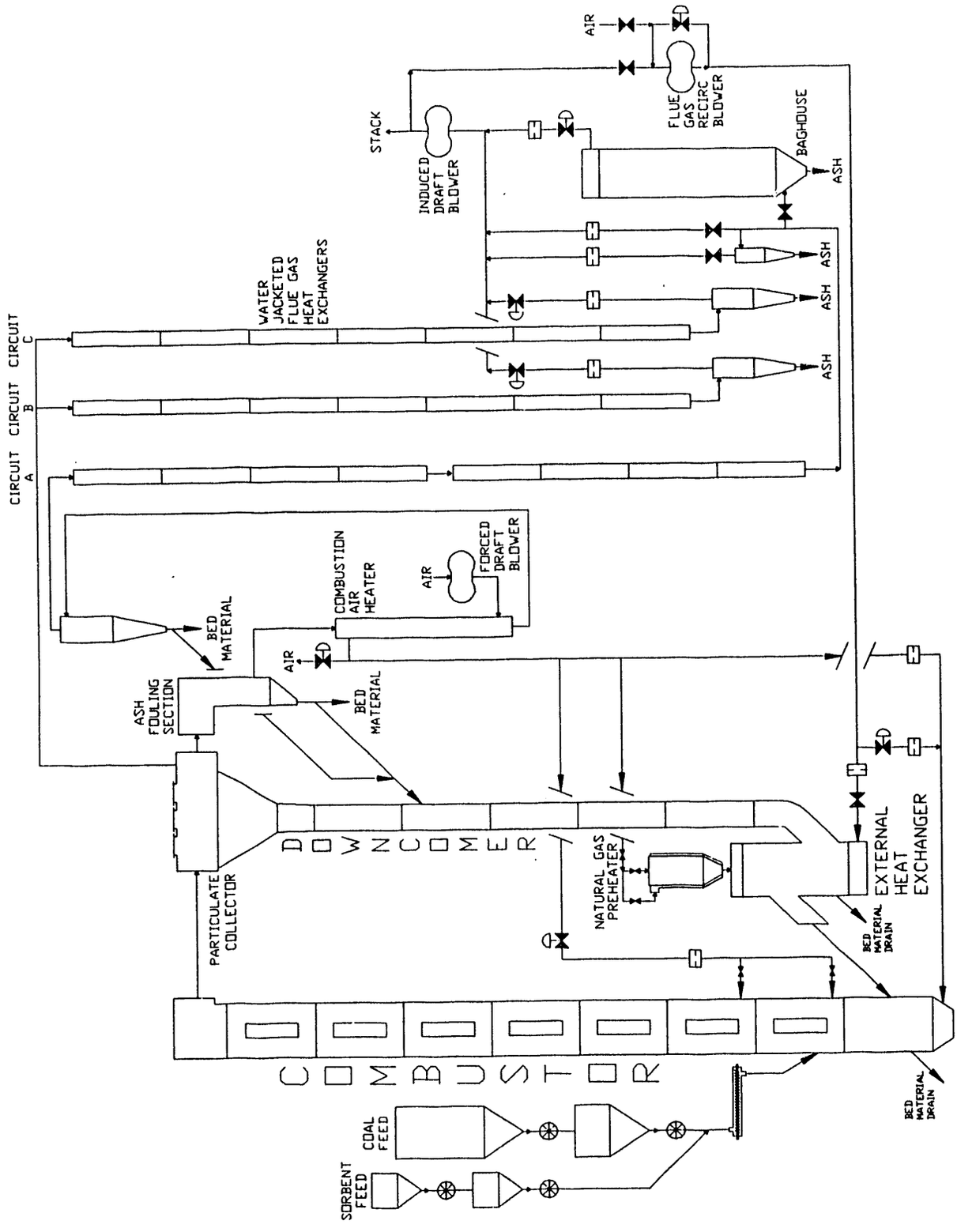

Figure 1. Schematic of CFB pilot plant

- Combustor Heat Exchange System,
- External Heat Exchange System, and
- Flue Gas Cooling Water System.

A forced draft blower supplies the combustion air and secondary air to the combustor. The combustion air heater is a shell and tube heat exchanger that uses hot flue gas to preheat the combustion air before it enters the combustor. Total combustion air flow is controlled by the amount of bypass through the combustion air bypass valve located directly after the combustion air heat exchanger. The secondary combustion air control valve determines the ratio of combustion air above the distributor plate to the amount of combustion air introduced into the combustor plenum below the distributor plate. The secondary combustion air can be introduced through manifolds at two different levels, located 5'-9" and 10'-6" above the distributor plate in Sections 2 and 3, respectively, of the combustor. There are four 3-inch manual gate valves at each level used to select where secondary air is introduced into the combustor.

Flue gas can be routed through any of three circuits, designated A for the primary circuit and B and C for the others. Flue gas flow during this test was entirely through Circuit A. Flue gas in Circuit A flows through the center duct of the particulate collection device, the ash-fouling section, the combustion air heater, an 18-inch cyclone, eight water-jacketed flue gas heat exchangers, and finally through either the flue gas bypass, the baghouse, or partially through a 10-inch cyclone. Circuits B and C, designed to be used for testing at higher gas flow rates, have seven water-jacketed flue gas heat exchangers and 14-inch cyclones for particulate collection. There are flow control valves at the exit of both cyclones in Circuits B and C, as well as gate-type isolation valves located at the entrance of Circuits B and C in the combustor exit. Temperatures and pressures are monitored throughout each circuit. The flue gas ducting for the three circuits combines and feeds into the induced draft (ID) blower. The ID blower is controlled with an electronic speed controller.

The flue gas recirculation blower is used to supply either air or flue gas to the external heat exchanger (EHX) and to supply flue gas to the combustor for flue gas recirculation testing. Manual gate valves before the blower select either air or flue gas to the blower. Air was used as the fluidizing gas during this testing.

Primary and secondary combustion air flow, fluidizing gas to the external heat exchanger, combustor flue gas recirculation, and flue gas flow rates are measured using orifice plates. Pressure transmitters and thermocouples interface with the data acquisition/control system to record and display the flow rates. Orifice differential and static pressures are also monitored with magnehelic pressure gages.

The ash-fouling section is connected to the Duct A exit of the particulate collection device. There are provisions for the installation of probes to be used for measurement of potential slagging, ash deposition, and/or ash fouling that could occur in the convective pass of a circulating fluidized-bed boiler.

The configurations of the coal and sorbent feed systems are the same. The coal storage hopper capacity is about 3000 lbs, while the sorbent storage

hopper capacity is about 500 lbs. Both have rotary valves below the storage hoppers feeding into weigh hoppers suspended from electronic weigh cells. Capacities of the coal and sorbent weigh hoppers are approximately 1000 and 500 lbs, respectively. At the bottom of the weigh hoppers, rotary valves, controlled with electronic speed controllers, are used for controlling the feed rates. At the exit of the weigh hopper rotary feed control valves, the coal and sorbent feed into a 3-inch auger that conveys the coal and sorbent mixture to the combustor. At this point, the mixture drops downward through a 3-inch pipe and feeds by gravity into the combustor.

The combustor is made up of a series of refractory-lined sections bolted together. Each section has two inches of hard abrasion-resistant refractory used in combination with seven inches of insulating refractory. The combustor plenum section contains the primary combustion air entrance and a bed material drain. A removable stainless steel nozzle distributor plate is installed between the plenum and the first combustor section. The solids recirculation return from the external heat exchanger enters the combustor at the first combustor section (Section 1). The next seven sections (Sections 2-8) each have two doorways on opposite sides for the installation of either blank refractory doors or heat exchange panels. At this time, eight of the possible fourteen heat exchange panels are installed in the combustor, two each in Sections 2 and 8, and none in section 5. Coal and sorbent feed enters the combustor at Section 2, which also contains the first set of secondary combustion air ports. The second set of four secondary combustion air ports enters the combustor at Section 3. Section 9, the combustor exit, connects to the particulate collection device. Thermocouple and pressure taps are present in all of the combustor sections.

The refractory-lined components of the solids recirculation system include the particulate collection device (PCD), the downcomer, and the external heat exchanger (EHX). The PCD is divided by refractory walls into three ducts. Duct A is in the center, with Ducts B and C on either side. Ducts B and C were not used during this test burn. There are nine removable refractory doors in the top of the collector, three in each duct. Chevrons are installed in Duct A for the collection of solids entering from the combustor exit. Solids captured in the PCD enter the downcomer and travel downward into the EHX. Additionally, solids collected in the ash-fouling section hopper and by the 18-inch cyclone also flow by gravity to the downcomer.

The EHX has a plenum section where air or flue gas is introduced. A removable stainless steel nozzle distributor plate is installed between the plenum and the main section of the EHX. A natural gas-fired preheater, described later, is attached to the top section of the EHX. Twenty U-shaped stainless steel water-cooled heat exchanger tubes are installed in a removable refractory-lined door in the EHX. There are thermocouples at the entrance and exit of each duct of the PCD. There are thermocouples and pressure taps distributed along the length of the downcomer and in the external heat exchanger.

The preheater combustion chamber is constructed with inner and outer stainless steel shells. The natural gas-fired burner is bolted on top of the preheater and fires downward. To maintain the inside metal surface of the preheater at an acceptable operational temperature, air is circulated through a baffled cooling jacket. Cooling air enters at the top of the preheater and

continues downward where it combines with the combustion gases at the bottom of the preheater transition cone. Preheater combustion air and the cooling jacket air are supplied by the forced draft blower. A butterfly valve in the 4-inch supply line from the FD blower isolates the system when it is not being used. There are butterfly valves in the combustion air and cooling air lines for control purposes. There are also orifice plates in each line with magnehelic pressure gages to monitor the flow rates. Gas flows to the natural gas burner and pilot burner are controlled with flowmeters located in the control room. There is also a flame safety system located in the control room to shut off the flow of natural gas to the preheater if 1) a flame is not present in the preheater, 2) combustion air is not being supplied to the preheater or cooling jacket, or 3) the combustion air pressure is greater than the natural gas pressure supplied to the preheater.

The water flow rate for all combustor heat exchangers is measured individually by flowmeters and controlled by the globe valves installed above the flowmeters in the panel boards. Total flow is measured by an in-line turbine flowmeter with a bypass around it to allow for maintenance or repair during operation. An air system is connected to the inlet manifolds of each of the heat exchange panels. Air is used to cool the heat exchanger panels during operation prior to the introduction of water. Each inlet manifold has a selector switch to allow for the proper distribution of either air or water through the manifold into the heat exchange tubes of the panels.

There are twenty heat exchangers installed in the external heat exchanger door. Each U-shaped heat exchanger is constructed out of 1-inch stainless steel pipe with 1/2-inch stainless steel tubing at each end. Each of eight circuits have a flowmeter and flow control valve mounted in a panel board to monitor and control the flow of water. Total flow is measured by an in-line turbine flowmeter with a bypass around it to allow for maintenance or repair during operation. Four different configurations are used, two using a single tube, two with two tubes in series, two with three tubes in series, and two with four heat exchange tubes connected in series. The temperature of the water exiting each circuit is measured by thermococouples.

2.2 Flue Gas Emission Monitoring

Flue gas composition was monitored continuously throughout the run. The results of these analyses were recorded by the data acquisition system, as well as displayed in the control room. Table 1 shows the instrument and technique used for each flue gas component. The flue gas analyzers were calibrated about three times a day

2.3 Analytical Equipment and Procedures

The following equipment and procedures were used for the analysis of coal, fly ash, limestone, and bed material samples:

- Proximate analysis was performed to determine moisture, ash, volatile matter, and fixed carbon levels of the coal. Moisture, ash, and volatile matter contents were determined with a Fischer 490 coal analyzer. Fixed carbon was calculated by subtracting the summation of percentage moisture, ash, and volatile matter from 100.

TABLE 1

Flue Gas Analytical Instrumentation

Gas Component	Analyzer	Detection Technique
O_2	Beckman Model 755	Paramagnetic
SO_2	Dupont Model 400	Photometric light absorption
NO_x	Thermo-Electron Series 10	Chemiluminescent in a photomultiplier tube
N_2O	Siemens Ultramat 5E	Infrared
CO, CO_2	Beckman Model 865	Infrared

- Ultimate analysis was performed to determine the carbon, hydrogen, nitrogen, sulfur, ash, and oxygen content of the coal. A Perkin-Elmer Model 240 elemental analyzer was used to determine CHN concentrations. Total sulfur content was determined with a Fischer sulfur analyzer. Ash was determined as described above in the proximate analysis. Oxygen was calculated by subtracting from 100 the sum of percentages of moisture and the other components of the ultimate analysis.

- Heating (calorific) value of the coal was measured by ASTM Method D 2015-77 using a Parr adiabatic calorimeter and master controller.

- Particle-size distributions of the coal, limestone, bed material, downcomer material, and baghouse ash were determined by sieve analysis according to ASTM Method D 410-38 utilizing U.S. standard screens. Wet sieve, Malvern (particle-size distribution by laser light scattering), and Coulter Counter analyses were also performed on the ash and limestone.

- Major mineral oxides (Al, Si, Na, Mg, Ca, P, K, Fe, Ti, and S) were determined by x-ray fluorescence using a Kevex 0700 x-ray spectrometer.

- The amount of carbonate (uncalcined limestone) in fly ash samples was determined by ASTM Method D 1756-62.

3.0 TEST MATRIX

The matrix of test parameters is shown in Table 2. The calcium-to-sulfur ratio shown in the table includes calcium in the coal as well as in the limestone. Test 1 was performed at full load with no limestone addition to establish baseline sulfur emission data for the Salt Creek coal. Test 2 is a full load test with the addition of limestone for sulfur capture. Tests 3 and 4 were partial load tests, based on coal feed rate. In both partial load tests, the temperature and superficial gas velocity were allowed to decrease,

TABLE 2

Test Parameters for Salt Creek Coal on CFBC

Test #	Temperature (°F)	Load (%)	Ca/S	Excess Air (%)	PA/SA	Velocity (ft/sec)
1	1616	100	0.54	20	54:46	16
2	1616	100	2.04	20	54:46	16
3	**	75	2.04	20	56:44	**
4	**	50	2.04	30	**	**
5	1475	100	1.54	45	70:30	16
6	1475	100	1.54	15	50:50	16
7	1625	100	1.54	15	70:30	16
8	1625	100	1.54	45	50:50	16
9	1625	100	3.54	45	70:30	16
10	1625	100	3.54	15	50:50	16
11	1475	100	3.54	15	70:30	16
12	1475	100	3.54	45	50:50	16

the excess air was not controlled, and the total heat-transfer surface in the combustor and external heat exchanger was held constant.

Tests 5 through 12 were all full load tests. Temperature, Ca/S ratio, excess air level, and primary-to-secondary air split were varied to determine their effects on flue gas emissions and combustion efficiency. High and low values of each parameter were tested; significant effects of any parameter will suggest more extensive testing of that parameter at a later date.

4.0 COAL AND LIMESTONE PROPERTIES

Salt Creek coal and limestone were provided by EPRI. The coal was crushed and sized to -1/4". A sample of the coal was taken during crushing and grinding, and samples were obtained during each test period. These samples were submitted for proximate, ultimate, and sieve analysis of the fuel, and determination of the major mineral oxides in the fuel ash were by x-ray fluorescence. Table 3 lists the results of the coal, mineral, and computer-controlled scanning electron microscope (CCSEM) analyses for each test period. The moisture ranged from 6.8 to 8.2%; the ash content ranged from 16.9 to 20.2%. The heating value, which ranged from 9976 to 10,563 Btu/lb for the EERC tests, was a bit lower than the 11,100 Btu/lb observed at the Nucla station. The average particle-size distribution of the coal is shown in Figure 2.

Table 3 shows values for sulfur in the coal, ranging from 0.40% to 0.50%, and adjusted sulfur in the coal, ranging from 0.49% to 0.57%. The adjustment was made for two reasons: first, the original sulfur levels were significantly lower than the average 0.54% sulfur in the coal at the Nucla station, and second, the original sulfur values were not consistent with the sulfur retention values calculated during the tests. The sulfur emissions from Test 1, with no limestone feed, were used as the baseline to determine what the sulfur content should be; sulfur was adjusted upward until the calculated sulfur retention for Test 1 was greater than zero, then the sulfur

TABLE 3

Coal Analyses (CFB-SC1-0191)

	Test Number												
	1	2	3	4	5	6	7	8	9	10	11	12	Average
Proximate Analysis (as-received), %													
Moisture	6.8	7.9	7.8	7.5	6.8	7.8	7.8	7.5	8.2	7.9	7.9	7.9	7.65
Volatile Matter	31.9	31.1	30.9	30.8	31.6	30.6	31.5	30.2	30.2	30.8	31.3	31.7	31.04
Fixed Carbon	44.7	42.1	42.3	41.6	43.1	42.4	43.4	42.1	43.0	42.7	43.1	42.4	42.74
Ash	16.9	18.9	19.0	20.1	18.5	19.1	17.3	20.2	18.6	18.6	17.7	17.9	18.58
Ultimate Analysis (as-received), %													
Carbon	60.4	57.7	57.6	57.7	59.6	58.9	59.9	58.2	58.7	59.0	59.7	58.7	58.82
Hydrogen	5.3	4.9	5.0	5.2	5.3	5.0	5.0	4.9	4.7	5.0	4.7	4.9	4.98
Nitrogen	1.3	1.2	1.1	1.1	1.1	1.2	1.2	1.1	1.1	1.1	1.1	1.1	1.15
Sulfur	0.43	0.41	0.41	0.41	0.41	0.40	0.41	0.50	0.44	0.46	0.46	0.48	0.48
Adjusted Sulfur	0.52	0.52	0.50	0.49	0.50	0.49	0.50	0.57	0.52	0.53	0.53	0.55	0.52
Oxygen	15.6	6.8	6.8	15.5	15.1	15.4	16.2	15.2	16.5	15.9	16.3	16.9	16.02
Ash	16.9	18.9	19.0	20.1	18.5	19.1	17.3	20.2	18.6	18.6	17.7	17.9	18.58
Ash Composition (% as oxides)													
Calcium, CaO	1.5	1.6	1.5	1.4	1.4	1.1	1.6	1.2	1.2	2.7	1.2	1.6	1.50
Magnesium, MgO	1.8	1.8	1.8	1.7	1.6	0.7	1.7	1.8	1.8	1.1	1.1	1.1	1.50
Sodium, Na_2O	0.5	0.2	0.4	0.0	0.0	0.6	0.3	0.6	0.2	0.0	0.0	0.0	0.23
Silica, SiO_2	59.3	58.9	57.8	57.7	59.1	67.9	59.0	58.7	57.6	60.5	62.8	59.8	59.93
Aluminum, Al_2O_3	31.4	30.9	31.1	31.1	31.5	33.3	31.4	31.3	31.3	28.6	29.6	29.1	30.88
Ferric, Fe_2O_3	2.7	2.8	3.1	2.8	2.6	2.2	2.0	2.3	2.1	2.7	2.4	8.5	3.02
Titanium, TiO_2	1.2	1.1	1.1	1.1	1.1	0.7	1.2	1.1	1.2	1.1	1.2	1.2	1.11
Phosphorous, P_2O_5	0.5	0.5	0.4	0.4	0.4	0.8	0.4	0.6	0.7	0.0	0.0	0.0	0.39
Potassium, K_2O	0.9	1.0	0.9	1.0	0.9	0.9	0.9	1.0	0.9	1.0	1.0	1.0	0.95
Sulfur, SO_3	0.9	1.1	1.0	0.9	0.9	0.5	1.0	1.2	1.2	0.8	0.7	1.3	0.96
High Heating Value (moisture-free), Btu/lb													
	10,563	10,013	10,084	9976	10,421	10,258	10,445	10,228	10,307	10,175	10,544	10,279	10,274

(continued)

TABLE 3 (continued)

Coal Analyses (CFB-SC1-0191)
Mineral Analysis (wt%)

	Size Fraction, microns						
	1.0 to 2.2	2.2 to 4.6	4.6 to 10.0	10.0 to 22.0	22.0 to 46.0	46.0 to 100.0	Totals
Quartz	0.1	0.2	1.0	1.4	2.0	3.2	8.0
Iron Oxide	0.0	0.0	0.0	0.2	0.1	0.5	0.8
Rutile	0.0	0.0	0.0	0.0	0.0	0.0	0.1
Alumina	0.0	0.0	0.0	0.0	0.0	0.0	0.0
Calcite	0.0	0.0	0.0	0.1	0.1	0.0	0.3
Dolomite	0.0	0.0	0.0	0.1	0.1	0.0	0.2
Ankerite	0.0	0.0	0.0	0.1	0.0	0.0	0.1
Kaolinite	1.1	5.2	20.1	6.6	12.0	13.3	58.4
Montmorillonite	0.4	1.2	1.6	1.7	3.3	3.1	11.3
K Al-Silicate	0.1	0.1	0.1	0.2	1.0	0.2	1.6
Ca Al-Silicate	0.0	0.1	0.0	0.0	0.0	0.0	0.1
Aluminosilicate	0.1	0.1	0.2	0.6	1.4	4.9	7.4
Mixed Al-Silicate	0.1	0.1	0.0	0.1	0.1	0.0	0.5
Pyrite	0.0	0.0	0.0	0.0	0.0	0.0	0.1
Apatite	0.0	0.0	0.0	0.1	0.0	0.0	0.1
Gypsum/Al-Silicate	0.0	0.1	0.0	0.0	0.0	0.0	0.1
Si-Rich	0.1	0.2	0.0	0.8	1.9	3.1	6.1
Ca-Rich	0.0	0.0	0.2	0.0	0.1	0.0	0.4
Unknown	0.3	0.4	0.6	0.6	1.5	1.2	4.6
Total	2.4	7.8	23.9	12.7	23.8	29.4	100.0

content for the rest of the tests was adjusted upward by the same percentage. The reason for the inaccurate sulfur analyses is under investigation.

The average elemental analysis for the limestone is shown in Table 4. The limestone used for these tests had a calcium content of 37% and no magnesium, compared to 36.3% calcium and 0.53% magnesium in the limestone used during the Nucla testing. The limestone was crushed and sized at the Nucla station prior to shipping to EERC. The limestone particle-size distributions from test to test were consistent; however, there was a great deal of variability in particle size depending on the method of analysis, as shown in Figure 3. The limestone was extremely cohesive and tended to agglomerate when subjected to vibration, such as that used in the sieve analyses. Subsequently, both Malvern and Coulter Counter tests were performed, and uniform results were obtained which were more consistent with the visual inspection of the limestone. The limestone used at Colorado Ute was sized by dry sieve analysis; Figure 3 shows the size distribution similarity between the EERC and Colorado Ute limestones.

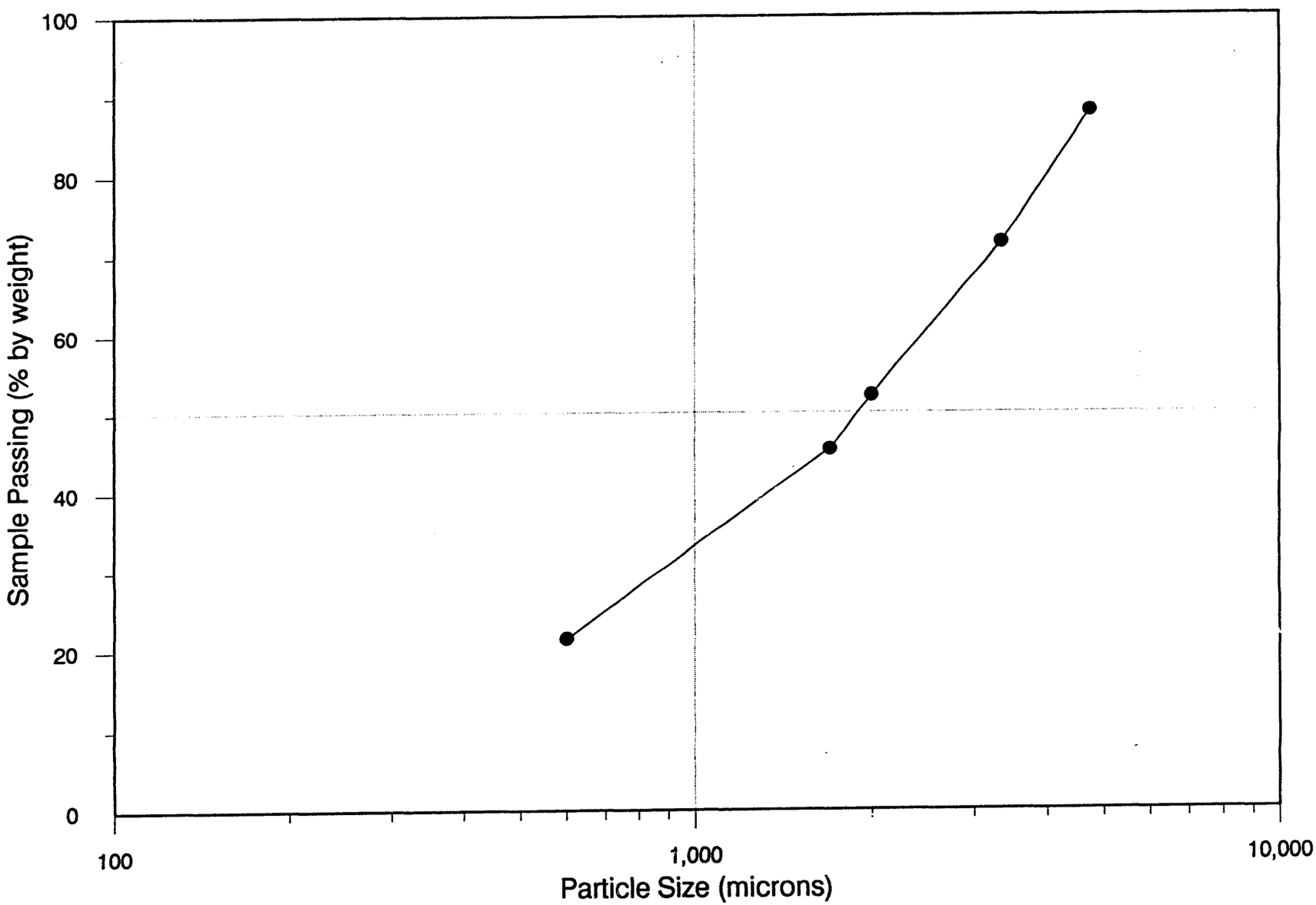

Figure 2. Size distribution of Salt Creek coal.

TABLE 4

Average Limestone Analysis (% ELEMENTAL)

Component	Average
Silica	1.8
Aluminum	0.3
Iron	0.2
Calcium	37.0
Magnesium	0.0
Sulfur	0.1

5.0 OPERATIONAL PERFORMANCE

5.1 Summary of Results

Upon completion of the run, data for each of the steady-state test periods were averaged. A summary of the process data for each test is presented in Table 5. The twelve test periods correspond to those presented in the test matrix listed in Table 2.

In general, the unit performed within the parameters specified in the original test plan. One notable exception was the actual calcium-to-sulfur ratio which was calculated at the conclusion of the run. The calcium-to-sulfur ratio was typically higher than specified in the test matrix. This can be attributed to limestone feed problems which will be discussed, along with specific results, in subsequent sections.

5.2 General Operability

The unit performed well during testing of the Salt Creek coal. No major problems were encountered with the unit or auxiliary equipment. The coal was crushed and sized to -1/4 inch and placed into storage hoppers. A rotary valve was used to transfer the coal from the storage hopper into the 1000-pound main feed hopper as needed. The feed hopper was suspended from a load cell to determine the coal feed rate. A second rotary valve was used to feed and meter the coal to a horizontal screw feeder. In addition to controlling the coal feed rate, the rotary valves serve to isolate the feed hoppers from system pressure in the combustor. Isolation is necessary to prevent possible ignition of the coal before it reaches the combustor, as well as to maintain stable feed rates and weigh cell measurements. The horizontal screw feeder conveyed the feed material to a section of 3" pipe, vertical at the top and entering the combustor at an angle of approximately 30° from vertical. Coal and limestone feed by gravity through this pipe. An air lance was used to assist the flow of material through the angled section of the gravity feed leg.

The limestone, crushed and sized prior to shipping and supplied along with the Salt Creek coal, was transferred to a 500-pound capacity storage hopper. The configuration of the limestone feed system was identical to the fuel feed side, and metered limestone flowed by gravity to the horizontal screw feeder where it combined with the feed coal. Some minor problems were encountered with the screw feeder due to binding. Additional minor problems

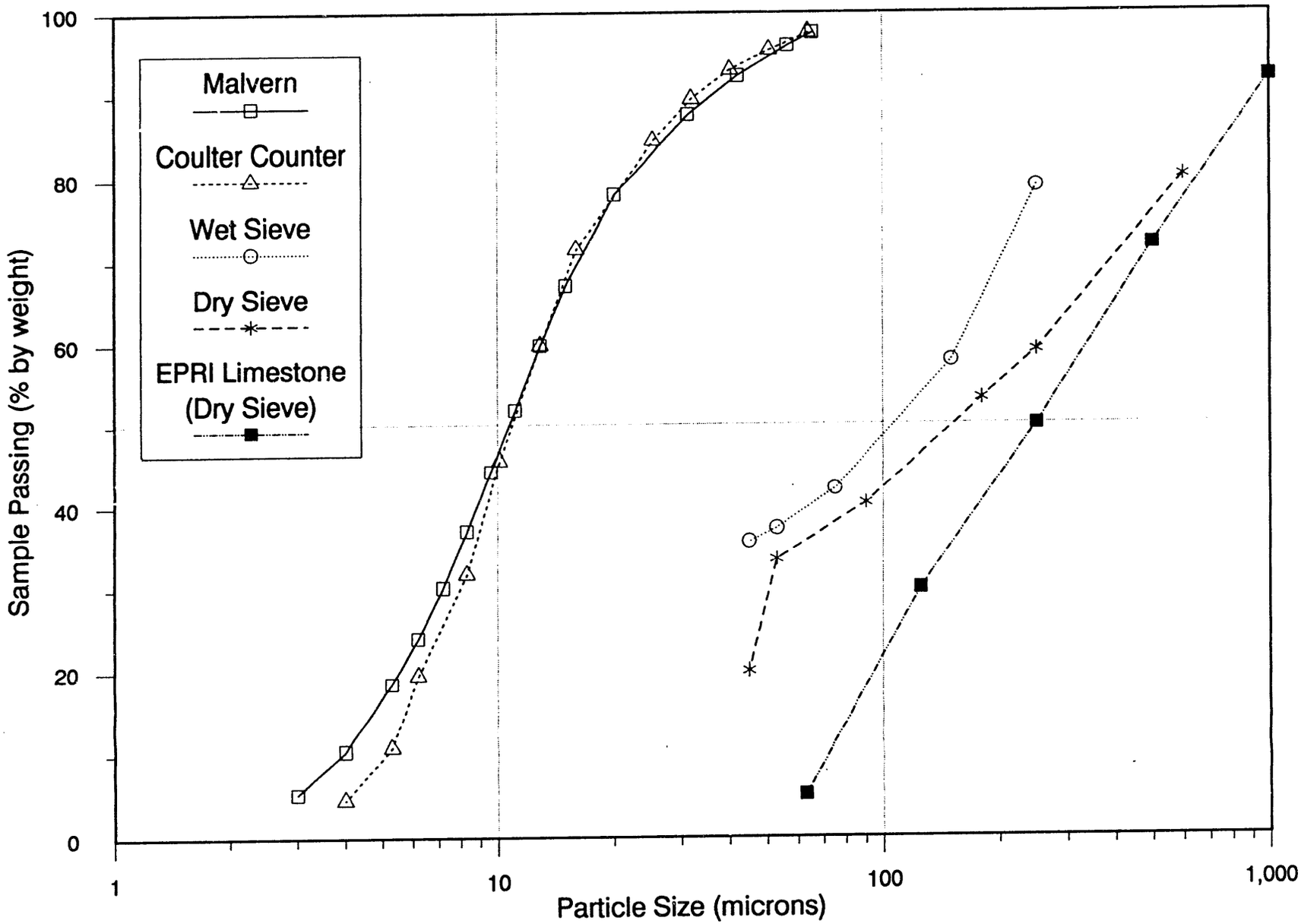

Figure 3. Size distribution of Salt Creek limestone (Test 2) using several analyses.

TABLE 5

Summary of Process Data

Test #	1	2	3	4	5	6	7	8	9	10	11	12
Date	1/22/91	1/23/91	1/23-24/91	1/24/91	1/25/91	1/29-30/91	1/30/91	1/30/91	1/30/91	1/31/91	1/31-2/1/91	2/1/91
Time	0830-1230	0045-1237	2022-0052	1230-2030	0300-0700	2230-0230	0535-0930	1230-1630	2128-2323	1015-1415	2015-0015	0400-0800
Coal Feed Rate (lb/hr)	226	239	204	133	213	258	237	208	208	245	263	215
Limestone Feed Rate (lb/hr)	0.0	9.1	6.2	4.5	6.3	3.4	8.6	9.0	5.1	12.8	16.4	15.3
Solids Recirculation Rate (lb/hr)	7658	11,965	11,246	2777	15,754	9577	14,563	9292	12,477	11,838	12,012	13,124
Combustion Air:												
EHX Flow (scfm)	47	56	52	59	37	46	47	55	54	54	50	52
Primary Air (scfm)	214	182	222	134	320	191	281	200	313	181	311	193
Secondary Air (scfm)	225	243	146	143	161	254	143	235	142	255	154	261
Feed Assist Air (scfm)	37	37	37	37	37	26	26	26	26	26	26	26
DC Aeration Air(scfm)	12.5	12.5	12.5	12.5	12.5	12.5	12.5	12.5	12.5	12.5	12.5	12.5
PA/SA (%)	0.51	0.47	0.61	0.53	0.65	0.47	0.67	0.51	0.69	0.47	0.67	0.47
Total Air (scfm)	535	531	469	385	568	530	510	529	547	528	554	546
Excess Air (%)	20.9	21.7	23.6	54.4	43.9	17.1	18.8	40.8	46.1	20.5	17.2	46.2
FG SGV (ft/sec)	16.5	16.2	13.9	10.0	16.0	15.6	16.1	16.4	16.7	16.5	16.1	15.7
EHX SGV (ft/sec)	1.7	2.2	2.0	1.8	1.4	1.6	1.9	2.2	2.2	2.1	1.7	1.9
Flue Gas:												
Flow Rate (scfm)	484	497	436	412	600	490	474	520	503	520	620	601
Oxygen (%)	3.65	3.76	4.00	7.40	6.44	3.11	3.35	6.12	6.65	3.60	3.10	6.63
SO_2 (ppm)	511	173	133	139	136	210	223	162	21	91	45	35
CO (ppm)	50	53	65	145	75	120	50	50	45	45	95	70
NO_x (ppm)	137	150	110	39	75	31	113	161	216	139	55	123
N_2O (ppm)	145	136	180	325	251	217	112	120	135	120	222	232
Ash:												
Bottom Ash Discharge Rate (lb/hr)	0	21	31	21	13	13	0	10	0	10	0	11
Combustor Ash Unburned Carbon (%)	0.34	0.33	0.40	1.34*	0.70	1.49	0.52	0.37	0.25	0.70	0.84	0.78
Downcomer Ash Unburned Carbon (%)	0.06	0.08	0.05	0.42	0.24	0.44	0.21	0.07	0.10	0.22	0.36	0.43
Cyclone Ash Discharge Rate (lb/hr)	0	24	4	0	42	20	5	10	37	8	40	19
Cyclone Ash Unburned Carbon (%)**	10.34	8.90	5.86	4.82	9.94	17.98	9.48	4.71	6.82	12.24	17.82	7.83
Baghouse Ash Dishcarge Rate (lb/hr)	12	37	17	10	24	20	21	14	21	26	23	10
Baghouse Ash Unburned Carbon (%)	10.34	8.90	5.86	4.82	9.94	17.98	9.48	4.71	6.82	12.24	17.82	7.83
Total Ash (meas., lb/hr)	12	82	52	31	79	53	26	34	58	44	63	40
Total Ash (calc., lb/hr)	38	52	44	30	44	52	47	48	49	55	58	49
Bottom Ash/Total Ash (meas., %)	0.0	25.6	59.6	67.7	16.5	24.5	0.0	29.4	0.0	22.7	0.0	27.5*

(continued)

TABLE 5 (continued)

Test #	1	2	3	4	5	6	7	8	9	10	11	12
Date	1/22/91	1/23/91	1/23-24/91	1/24/91	1/25/91	1/29-30/91	1/30/91	1/30/91	1/30/91	1/31/91	1/31-2/1/91	2/1/91
Time	0830-1230	0045-1237	2022-0052	1230-2030	0300-0700	2230-0230	0535-0930	1230-1630	2128-2323	1015-1415	2015-0015	0400-0800
Combustor Temperatures (°F)												
Plenum	599	598	550	421	601	590	655	588	639	618	627	568
Section 1	1596	1590	1544	1304	1449	1432	1608	1593	1579	1577	1447	1437
Section 2	1620	1619	1565	1331	1471	1462	1620	1602	1592	1603	1467	1454
Section 3	1627	1628	1573	1377	1485	1490	1639	1626	1605	1636	1498	1483
Section 4	1617	1626	1569	1382	1491	1499	1641	1625	1607	1634	1504	1486
Section 5	1629	1636	1579	1402	1497	1513	1649	1638	1613	1649	1513	1495
Section 6	1606	1623	1563	1378	1490	1507	1642	1623	1605	1636	1506	1487
Section 7	1595	1614	1554	1367	1482	1497	1633	1611	1597	1624	1498	1476
Section 8	1591	1621	1560	1369	1495	1513	1646	1626	1609	1638	1512	1492
Section 9	1611	1631	1571	1382	1498	1522	1652	1635	1612	1650	1519	1500
Combustor Exit	1608	1612	1559	1383	1490	1519	1645	1626	1600	1646	1513	1495
Average	1607	1613		1351	1476	1478	1630	1615	1596	1617	1485	1470
EHX Tempe-atures (°F)												
0.5' above dist. plate	1340	1438	1409	1048	1365	1206	1496	1505	1525	1420	1221	1324
1.5' above dist. plate	1339	1435	1412	1071	1358	1203	1489	1506	1526	1420	1210	1312
2.7' above dist. plate	1338	1430	1404	1064	1353	1191	1483	1495	1513	1409	1207	1319
3.8' above dist. plate	1218	1387	1343	1015	1247	1131	1428	1457	1482	1382	1156	1268
5.3' above dist. plate	1080	1270	1216	864	1100	995	1282	1322	1359	1268	1037	1138
Average	1339	1434	1406	1061	1358	1200	1489	1502	152[illegible]	1416	1214	1317
Downcomer Temperatures (°F)												
Section 3	1537	1532	1467	1199	1437	1443	1577	1544	1549	1561	1453	1427
Section 4	1527	1522	1459	1225	1425	1433	1577	1545	1548	1562	1447	1427
Section 6	1553	1562	1507	1319	1460	1470	1600	1577	1570	1588	1474	1459
Section 8	1571	1595	1536	1381	1476	1494	1621	1599	1588	1611	1492	1469
18" Cyclone Exit	731	772	697	550	731	729	756	728	737	750	698	688
Baghouse Inlet	467	382	444	334	350	358	408	410	417	317	320	385
Baghouse Outlet	392	321	365	272	289	311	344	346	356	269	273	326
ID Fan Inlet	316	253	275	196	210	261	296	294	303	234	225	261
Air and Gas Pressures												
Primary air (psia)	16.3	16.6	16.6	16.2	16.6	16.1	16.2	16.1	16.3	16.1	16.5	16.4
Secondary air (psia)	14.5	15.0	14.6	14.6	14.8	14.8	14.4	14.8	14.6	15.0	14.8	15.1
Combustor plenum (psia)	78.3	70.7	69.0	58.1	66.0	58.5	57.3	62.3	59.0	57.4	63.8	61.8
Comb. dP (in. H_2O)	49.7	43.7	55.9	44.8	29.0	43.3	42.4	38.4	37.9	40.1	40.4	46.2
Downcomer dP (in. H_2O)	30.5	51.2	29.1	33.2	25.9	21.2	19.[illegible]	12.3	15.4	11.5	14.5	13.2
18" Cyclone dP (in. H_2O)	2.7	2.1	2.0	1.3	2.4	2.0	2.4	2.3	3.5	1.7	2.2	6.0
Baghouse dP (in. H_2O)	7.6	4.7	3.3	2.4	3.4	5.5	5.1	4.9	6.0	3.9	4.2	3.3
Baghouse outlet (psia)	-12.8	-13.5	-13.7	-14.1	-13.5	-13.0	-12.8	-13.5	-13.0	-13.2	-13.5	-13.2

* Estimated value.
** The cyclone ash coal carbon content has been assumed to be equivalent to the baghouse ash coal carbon content.

arose due to blockage of feed material in the gravity feed leg beneath the auger. A somewhat more persistent problem was encountered with the flow of limestone out of the feed hopper. The crushed limestone had a very high angle of repose which caused frequent "rat-holing" and subsequent loss of sorbent feed. As a result, considerable attention had to be paid to the limestone feed hopper to maintain a continuous supply of sorbent to the combustor.

It is not anticipated that there would be any major coal feed problems unless there were significant differences in the surface moisture of the coal tested at EERC and that used at a commercial plant. Limestone feed may present some problems at a commercial CFB using a feed system similar to that employed at EERC. However, it is believed that minor design modifications would alleviate the limestone feed problems experienced during the EERC pilot plant test run.

One additional problem which surfaced during the course of testing was blinding of the baghouse bags over time. The combination of a relatively thick layer of ash on the baghouse bags with a high baghouse static pressure resulted in deformation of some of the bag cages and the development of a hole in at least one bag. The observed high pressure drops across the baghouse may be a function of the ash, considering the cohesive nature of the material. This could present problems in a commercial plant, but it is believed that minor adjustments in cage design and on-line bag cleaning procedures may alleviate the baghouse problems encountered during pilot-scale testing at EERC. Another area of concern with regards to the fly ash is the design of commercial ash-handling systems. Particular attention must be paid to the design of fly ash hoppers to compensate for the cohesiveness of the ash and allow for adequate removal during operation.

The pilot-scale CFB has nineteen thermocouples located along the length of the combustor in nine sections. Also, there are five thermocouples inplace along the length of the downcomer. During full-load testing, the temperature distribution throughout the combustor and downcomer was very uniform and, on the average, did not vary by more than 100°F, indicating good solids recirculation within the system. During partial load tests, the combustor temperature distribution remained fairly uniform. However, temperatures in the downcomer were up to 200°F lower than the highest combustor temperatures, as would be expected due to proportional heat loss through refractory-lined walls.

5.3 Collector Performance

Chevron collectors with internally sloped deflector plates were used in the particulate collection device during this test. The chevron collectors feature a geometry that helps force the particulate to the back of the collectors where there is an opening all the way down the back of the collector to allow the particulates to flow downward into the collection hoppers that feed into the downcomer. The particulate collection device housing the chevron collectors has three ducts into which the combustor exits. The main middle duct used during this test is referred to as Duct A while the outside two ducts are referred to as Ducts B and C. Ducts B and C can be brought on-line, if required, for higher velocity testing than is currently being conducted. Three stages of collectors were utilized in Duct A during this test. The first two stages are intended to capture the majority of particulate, while the third stage was designed with the intention of

capturing smaller particles. The first stage used four chevron collectors, two in each row. The second stage had a total of twelve chevron collectors, four in each row. The third stage had a single row of four chevron collectors using nozzles to accelerate the flow into them.

At the conclusion of the two weeks of testing, the three sets of collectors were removed for inspection. It appeared that all four collectors in stage one had been operating properly. In the second stage, the four collectors in the back row were plugged off with fine bed material, while the first two rows appeared to have been operating with some slight blockages at their top and bottom. The third stage of collectors were entirely plugged with bed material fines. The outer two nozzles on stage three had also warped, blocking much of the flow to these two collectors. It appears that a combination of factors caused plugging of the back row of stage two and all of the stage three collectors. All of these collectors are about half the size of the ones used in stage one, resulting in a smaller exit from the chevron collector into the collection hoppers. The collectors that definitely plugged up exit onto the back slope of the hopper they are over, allowing less volume for solids to flow through at their exit. Stage three nozzles forced all of the fines into these collectors, probably overloading this stage with more fines than they could handle.

Operational temperatures in the downcomer remained high throughout testing, indicating good collector performance even though approximately half of the chevron collectors were plugged for, at least, the latter portion of testing. Use of chevron collectors appears to have resulted in a collector that more closely simulates the operation of a large cyclone collector used for a CFB utility or industrial boiler. Additional testing should be conducted to better characterize the actual collection performance of the system.

The current design is not forgiving of the large amount of fines that were traveling through the system due to the addition of recycling the catch from the cyclone. Some of the plugging problems encountered might also have been more specific to the limestone used for this test, since the limestone was a smaller size than had been originally anticipated for operation with this pilot facility, and was extremely cohesive. To alleviate some of these problems, it is planned to replace the smaller chevrons previously used in stages two and three with larger chevron collectors similar to the stage one chevrons, increase the slope of the defector plates in the new collectors, increase the size of their back opening, and make allowances for chevron collectors that have their exits directly over the hopper side walls.

No problems have been encountered with the durability of the chevron collectors. They experienced more than 200 hours of high-temperature exposure at temperatures averaging approximately 1500°F and, on occasion, temperatures approaching 1700°F for short durations of a couple hours. The material of construction is 304 stainless steel. No apparent warpage is present, with many of the sharp edges only slightly dulled. The only damage that occurred was to the one-eighth-inch stainless steel sheet that was used to construct the nozzles for the third stage. This appears to be due to a combination of expansion and inadequate strength.

5.4 Recirculation Rates and Size Distributions

The solids recirculation rate was determined by calculating the heat balance around the external heat exchanger. The average solids recirculation rates for each test are shown in Table 6. While a lot of variability was evident in the calculated rate, the recirculation ratio was generally within the typical range of 40 to 80. The recirculation ratio is the ratio of solids recirculation rate to coal and sorbent feed rate. Some of the recirculation rates in Table 6 may appear quite low, while the corresponding recirculation ratio is relatively high. Test 1 had a very high recirculation ratio because no limestone was being fed during that test; consequently, the solids feed rate was lower than in the other tests. Test 4 had low coal and sorbent feed rates to achieve the 55% load condition; however, the low superficial gas velocity in the combustor produced a very low recirculation rate, with a correspondingly low recirculation ratio.

The cyclone collection efficiency for this unit was very good. The higher the cyclone efficiency, the greater the proportion of material that must be drained from the combustor bed as opposed to fly ash collected in the baghouse. In a commercial combustor, a cyclone collection efficiency of 99.0 to 99.5% or more is required to maintain sufficient solids in the system for stable operation. Consistency in the sulfur emissions, heat-transfer coefficient, and the temperature distribution in the combustor, downcomer, and external heat exchanger indicates uniform mixing and solids distribution throughout the system.

The particle-size distributions throughout the run were fairly consistent. Figure 4 shows the particle-size distribution in the downcomer for Test 1, Test 4, and the average of the remaining tests which were very similar. Test 1 had proportionally larger particles in the downcomer because it was performed early in the run and without limestone addition. Therefore, the bed was composed primarily of coal ash and relatively large start-up sand. Limestone was fed during Tests 2 through 12, which resulted in progressively smaller bed particle sizes as the bed turned over from predominantly silica sand and coal ash, to limestone and coal ash. The low velocity of Test 4 prevented larger particles from being carried out of the combustor, giving the smaller particle size shown in Figure 4. Figure 5 shows the particle sizes found in the combustor, downcomer, and baghouse during Tests 2 and 4.

5.5 Bottom Ash/Total Ash Split

An ash balance for each test period, along with averages for the entire run, is given in Table 7. Ash input to the system was composed of calculated quantities of coal ash and limestone ash. The limestone-derived ash was further broken down into estimates of the sorbent which either was calcined or had undergone sulfation. The output of ash from the CFB system was measured values of bottom ash (combustor and downcomer bed material), ash removed from the 18" cyclone, and baghouse ash (fly ash).

The bottom ash and cyclone ash outputs are reported as the difference between the amount of material removed and the amount of material added back to the system to maintain a good solids inventory. The negative output values of bottom ash and cyclone ash in Tests 1 and 4, respectively, are a result of this calculation method.

TABLE 6

Solids Recirculation and Heat-Transfer Data

Test	Temperature (°F)	Load (%)	Ca/S	Excess Air (%)	PA (%)	Solids Recirc. (lb/hr)	DC D_{50} (micron)	H_o (Btu/hr-ft²-°F)	Heat Flux (Btu/hr-°F)	Cyclone Effic. (%)	Recirc. Ratio
1	1606	100	0.3	21	51	7660	300	23.7	34,700	99.53	169
2	1614	100	2.5	22	47	11,960	210	21.0	30,900	99.38	47
3	1559	75	2.1	24	61	11,250	240	22.7	32,100	99.83	54
4	1351	50	2.4	54	53	2780	110	14.4	18,000	99.64	21
5	1476	100	2.1	44	65	15,750	220	20.5	24,700	99.58	72
6	1478	100	1.1	17	47	9580	240	22.0	29,700	99.58	37
7	1630	100	2.5	19	67	14,560	240	24.1	35,800	99.82	60
8	1615	100	2.5	41	51	9290	220	20.8	30,900	99.74	43
9	1597	100	4.4	46	69	12,500	270	23.1	33,600	99.54	57
10	1617	100	3.5	21	47	11,840	220	17.3	25,700	99.71	47
11	1485	100	3.7	17	67	12,010	250	19.8	26,700	99.48	43
12	1470	100	4.1	46	47	13,120	220	18.4	24,600	99.75	58

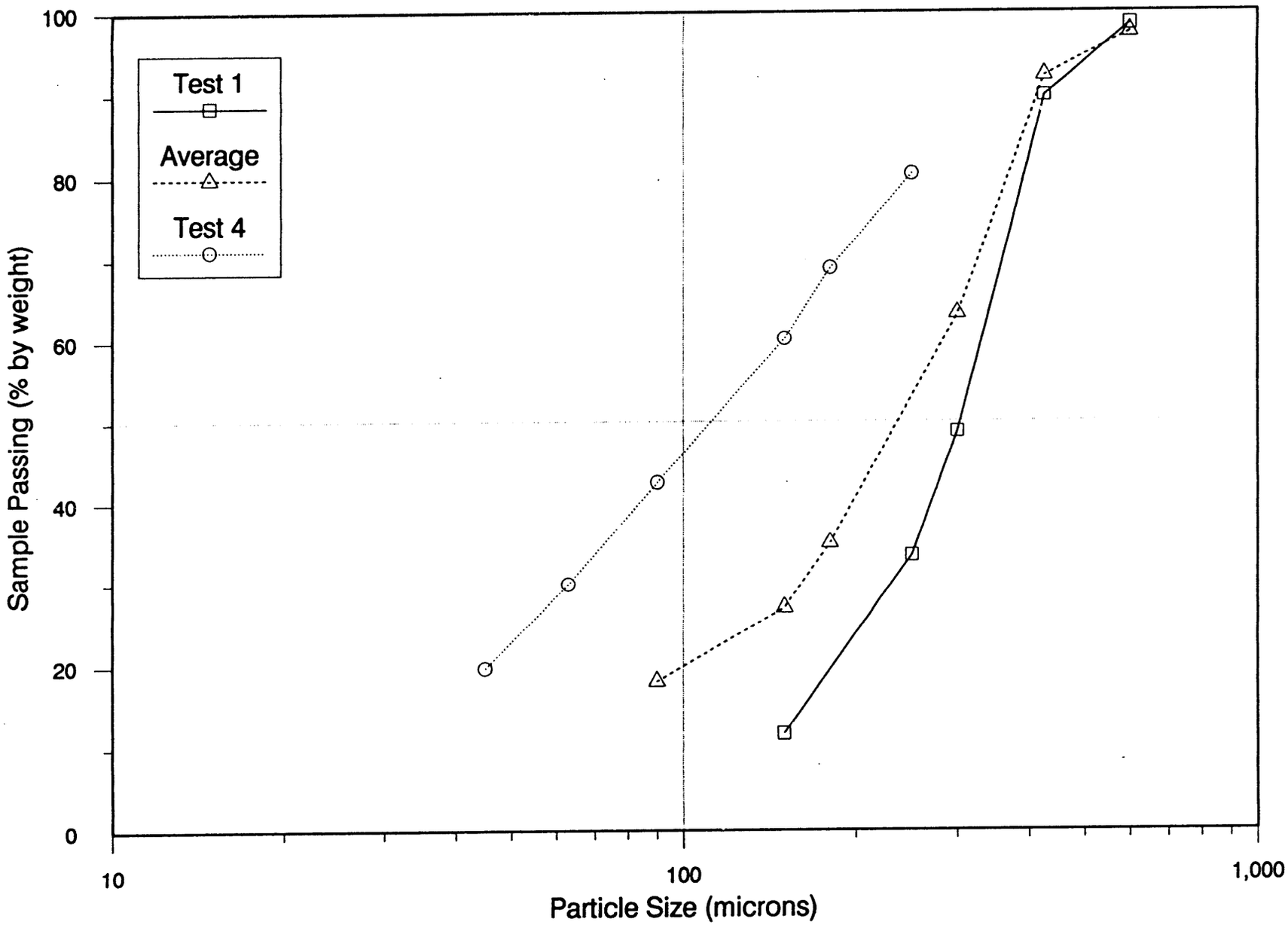

Figure 4. Size distribution of downcomer material for Tests 1 and 4, and the average of all tests.

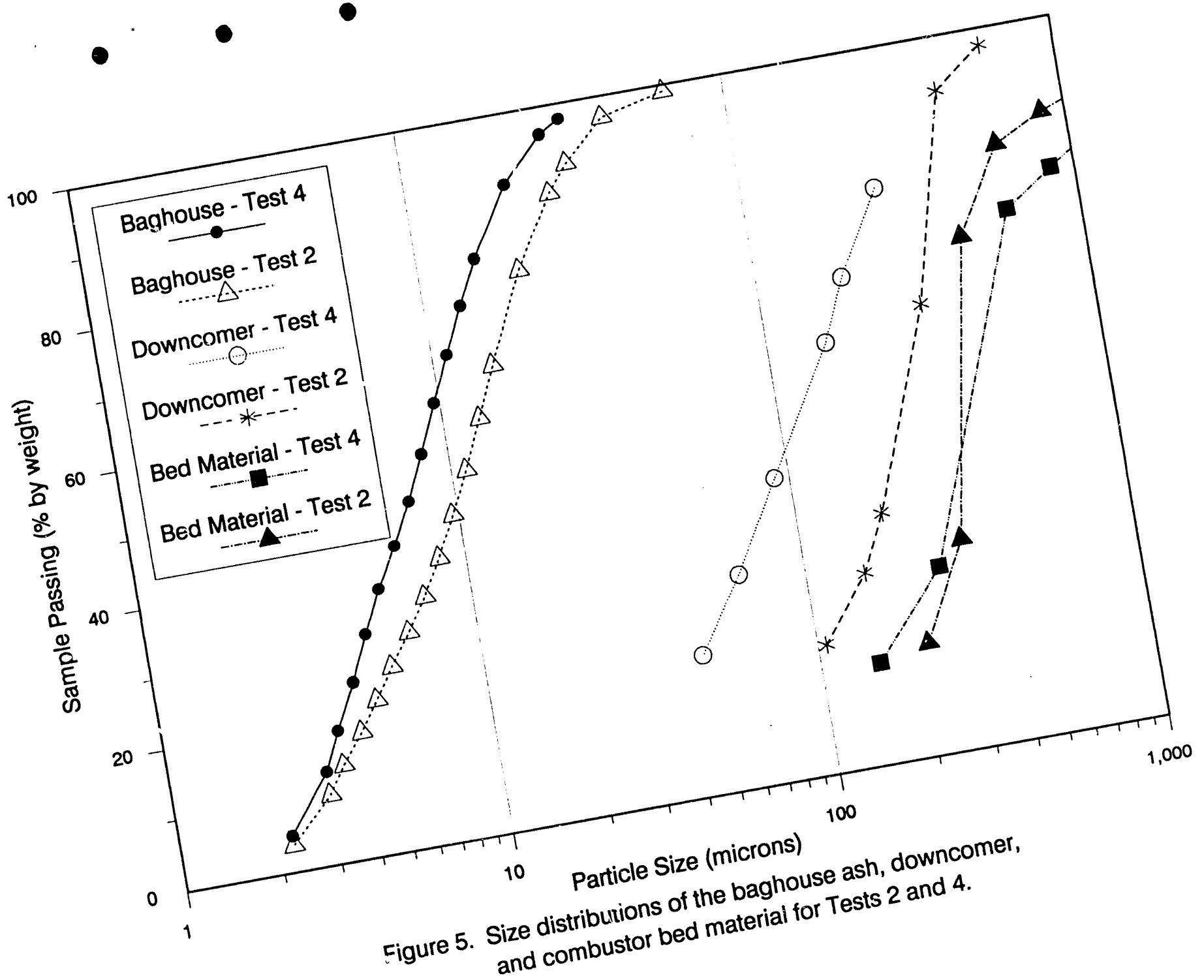

Figure 5. Size distributions of the baghouse ash, downcomer, and combustor bed material for Tests 2 and 4.

TABLE 7

Ash Balance

	Test Number												Run Average	Run Average W/O #1
	1	2	3	4	5	6	7	8	9	10	11	12		
Input (lb/hr):														
Fuel Ash	38	45	39	27	39	49	41	42	39	46	46	39	40.8	41.1
Sorbent Ash:*														
CaO	0	4	2	2	3	1	4	4	7	6	7	7	4.0	4.4
$CaSO_4$	0	3	3	1	2	2	2	2	3	3	4	4	2.4	2.6
Total Ash In (lb/hr)	38	52	44	30	44	52	47	48	49	55	58	49	47.2	48.0
Output (lb/hr):														
Bottom Ash	-38	9	3	12	0	13	0	10	0	21	0	11	3.4	7.2
Cyclone Ash	0	0	0	-6	35	20	5	10	37	8	40	19	13.9	15.2
Baghouse Ash	12	37	15	10	24	20	21	14	21	26	23	10	19.4	20.1
Total Ash Out (lb/hr)	-26	46	18	16	58	53	26	34	58	55	63	40	36.8	42.5
Closure (%)	-68.0	88.6	41.2	53.4	131.2	101.8	55.5	70.7	118.1	100.6	108.4	81.1	77.9	88.4
Bottom Ash/Total Ash (lb/hr)**	68.6	28.7	65.7	66.6	45.7	61.6	55.2	70.9	57.2	52.5	60.4	79.7	58.9	58.1
Coal Ash in Sample, %														
Combustor	17	35	37	45	42	50	37	35	--	54	52	53	--	--
Downcomer	13	45	46	69	59	49	32	--	--	72	68	69	--	--
Baghouse	98	87	92	96	80	81	86	93	74	85	81	87	--	--

* The CaO and $CaSO_4$ mass inputs are included to express sorbent equivalent mass inputs.
** The bottom ash-to-total ash ratio was calculated as [(Total Ash In - Baghouse Ash)/Total Ash In].

The ratios of bottom ash-to-total ash, as well as the percent closure, were calculated and are included in Table 7. The average closure for the entire run was about 78%, but increased to near 90% with Test 1 taken out of the average. The bottom ash-to-total ash split averaged approximately 59% for the run and varied from about 29% to 80%. Operation of the pilot plant at reduced load did not significantly affect the ash split. The problems encountered with fly ash cohesiveness may explain the high bottom ash-to-total ash ratios reported. The bottom ash-to-toal ash was calculated as the total ash input minus fly ash divided by the total ash. It is believed that significant quantities of fly ash were adhering to the baghouse bags and bottom hopper during various tests and may not have been properly accounted for during the run. When calculated as total ash minus bottom ash divided by total ash, a much lower bottom ash-to-total ash is indicated. The run average calculated by this method is 7.2%, and the average without test 1 is 15%. These numbers may be more representative of the ash split. More care must be taken in future tests to ensure a good ash balance closure.

6.0 THERMAL PERFORMANCE

6.1 Energy and Material Balances

The fuel, air, and flue gas balances were calculated, and the results are presented in Tables 8, 9, and 10, respectively. The theoretical fuel feed rate was calculated using actual fuel characteristics and measured O_2 and CO_2 concentrations. The theoretical air flow rate and flue gas rates were calculated using the actual coal feed rate and excess air levels. The measured fuel feed rates were all slightly higher than the calculated values, while the measured air flow rates were all lower than the calculated values. In both cases, the error was greatest in Test 6.

The energy balances for the twelve tests are presented in Table 11, both in Btu/hr and as percentages. The energy input was made up of the energy potential of the fuel, the primary and secondary combustion air, the external heat exchanger fluidizing air, and the energy released from the sulfation of the sorbent. Measurable heat loss sources were the combustor heat exchange doors, the external heat exchanger cooling coils, the flue gas, the unburned carbon in the ash removed, and the energy absorbed during calcination of the sorbent. The unmeasurable heat loss due to convection and radiation was obtained by difference. Almost half of the heat was removed by the flue gas, while 36% to 50% of the heat was removed through the combustor heat exchange doors and external heat exchanger cooling coils. Average wall losses accounted for about 11% of the total heat loss.

The material balances for the twelve test periods are shown in Table 12. The material balance closures were generally good, with the greatest deviation from complete closure occurring in Test 6 at 107.5%.

6.2 Combustion Efficiency

Combustion efficiencies for all twelve tests are shown in Table 13. The combustion efficiency calculation is based on the amount of unburned carbon removed in the bottom ash and fly ash as a function of the carbon input as coal feed and bed material addition.

TABLE 8

Fuel Balance

	Test Number											
	1	2	3	4	5	6	7	8	9	10	11	12
Fuel Feed Rate (meas., lb/hr)	226	239	204	133	213	258	237	208	208	245	263	215
Fuel Feed Rate (calc., lb/hr)	226	234	203	131	204	242	226	204	204	234	253	202
Error (%)	-0.1	2.1	0.6	1.1	4.1	6.2	4.5	2.2	2.0	4.6	3.5	5.8

Note: meas. = feed rate calculated by linear regression performed on coal feed hopper weight loss over time.
calc. = theoretical feed rate calculated on the basis of the coal analysis for each test period.

TABLE 9

Air Balance

	Test Number											
	1	2	3	4	5	6	7	8	9	10	11	12
Air Flow Rate (meas., scfm)	523	519	457	373	555	518	498	516	535	516	541	533
Air Flow Rate (calc., scfm)	522	528	459	379	579	564	533	539	557	551	573	577
Error (%)	0.1	-1.9	-0.6	-1.6	-4.4	-9.0	-7.1	-4.3	-4.2	-6.7	-5.9	-8.2

Note: meas. = the sum of the primary and secondary combustion air flows, EHX air flow, and coal feed and downcomer assist air.
calc. = theoretical air flow calculated on the basis of the coal analysis and measured coal feed rate for each test.

TABLE 10

Flue Gas Balance

	Test Number											
	1	2	3	4	5	6	7	8	9	10	11	12
Flue Gas Flow Rate (meas., scfm)	484	497	436	412	600	490	474	520	503	520	620	601
Flue Gas Flow Rate (calc., scfm)	556	562	488	399	612	600	566	569	587	585	608	609
Error (%)	-14.8	-13.0	-12.1	3.1	-2.0	-22.4	-19.4	-9.5	-16.7	-12.5	1.9	-1.3

Note: meas. = the flue gas flow measured during the run through an orifice located just upstream of the ID fan.
calc. = theoretical flue gas flow calculated on the basis of the coal analysis and actual coal feed rate for each test.

The combustion efficiencies for Tests 1 through 4 are shown as a function of bed temperature in Figure 6. Tests 1, 2, and 3 were performed at relatively low levels of excess air (21% - 24%), while the excess air in Test 4 was 54%. Tests 3 and 4 were low load tests, 85% and 55% respectively. The high calculated combustion efficiency for Test 1 can be attributed in part to the fact that no bottom ash was removed during the test, and the baghouse discharge rate was relatively low. During this test the unit was operated with a sand bed; limestone feed was not initiated until Test 2.

The expected trend of higher combustion efficiency with higher temperature is not seen for the first 4 tests (see Figure 6). The average superficial gas velocity for each test is given in Table 13. In Tests 3 and 4, the gas velocity was decreased from a nominal 16 ft/sec, to 13.9 and 10.0 ft/sec respectively. This impacts the system in two ways. The gas and

TABLE 11

Energy Balance

	Test Number											
	1	2	3	4	5	6	7	8	9	10	11	12
Input (Btu/hr) :												
Coal	2,097,669	2,074,464	1,783,809	1,152,685	1,948,758	2,299,451	2,152,662	1,855,265	1,860,143	2,163,830	2,417,206	1,920,840
Primary Air	123,283	106,263	118,806	51,717	187,190	109,821	179,660	116,994	196,645	108,090	191,592	104,544
Secondary Air	129,620	141,878	78,168	55,474	94,180	146,045	91,428	137,468	88,585	151,684	94,872	141,378
EHX Air	2334	3053	2591	3056	1197	2148	2194	2810	2698	2886	2450	2888
Sorbent Sulfation	0	4293	4100	2358	3954	2898	3394	3293	5487	5047	6685	5944
Total	2,352,907	2,329,951	1,987,474	1,265,290	2,235,280	2,560,363	2,429,339	2,115,830	2,153,558	2,431,536	2,712,804	2,175,595
Input (%):												
Coal	89.2	89.0	89.8	91.1	87.2	89.8	88.6	87.7	86.4	89.0	89.1	88.3
Primary Air	5.2	4.6	6.0	4.1	8.4	4.3	7.4	5.5	9.1	4.4	7.1	4.8
Secondary Air	5.5	6.1	3.9	4.4	4.2	5.7	3.8	6.5	4.1	6.2	3.5	6.5
EHX Air	0.1	0.1	0.1	0.2	0.1	0.1	0.1	0.1	0.1	0.1	0.1	0.1
Sorbent Sulfation	0.0	0.2	0.2	0.2	0.2	0.1	0.1	0.2	0.3	0.2	0.2	0.3
Total (%)	100.0	100.0	100.0	100.0	100.0	100.0	100.0	100.0	100.0	100.0	100.0	100.0
Output (Btu/hr):												
Flue Gas (sens.)	1,038,292	1,068,521	893,039	641,666	1,050,544	1,083,008	1,084,226	1,076,781	1,082,685	1,128,622	1,097,031	1,046,497
Ash (sens.)	4929	34,154	20,834	10,752	29,605	19,667	10,865	14,004	23,512	18,157	24,041	14,863
Ash (chem.)*, **	0	19,955	743	937	37,551	2,275	0	287	18,106	675	39,678	287
Combustor	722,750	642,735	668,453	375,062	569,979	617,398	745,640	643,279	698,326	534,654	555,823	511,223
EHX	364,474	308,529	95,966	69,676	326,456	643,546	307,714	102,626	105,989	451,646	794,916	321,681
Sorbent Calcination	0	6986	4711	3409	4833	2604	6565	6856	11,528	9805	12,562	11,720
Conduction and Radiation Losses	222,462	249,073	304,471	163,788	216,311	194,140	274,328	272,284	231,518	288,652	228,431	269,611
Total	2,352,907	2,329,951	1,987,474	1,265,290	2,235,280	2,560,363	2,429,339	2,115,830	2,153,558	2,431,536	2,712,804	2,175,595
Output (%)												
Flue Gas (sens.)	44.1	45.9	44.9	50.7	47.0	42.3	44.6	50.9	50.3	46.4	40.4	48.1
Ash (sens.)	0.2	1.5	1.0	0.8	1.3	0.8	0.4	0.7	1.1	0.7	0.9	0.7
Ash (chem.)*, **	0.0	0.9	0.0	0.1	1.7	0.1	0.0	0.0	0.8	0.0	1.5	0.0
Combustor	30.7	27.6	33.6	29.6	25.5	24.1	30.7	30.4	32.4	22.0	20.5	23.5
EHX	15.5	13.2	4.8	5.5	14.6	25.1	12.7	4.9	4.9	18.6	29.3	14.8
Sorbent Calcination	0.0	0.3	0.2	0.3	0.2	0.1	0.3	0.3	0.5	0.4	0.5	0.5
Conduction and Radiation Losses	9.5	10.7	15.3	12.9	9.7	7.6	11.3	12.9	10.8	11.9	8.4	12.4
Total (%)	100.0	100.0	100.0	100.0	100.0	100.0	100.0	100.0	100.0	100.0	100.0	100.0

* The heat of combustion coefficient for pure carbon is an average of values found in Perry's Chemical Engineering Handbook, Perry et al. (1984) and the Standard Handbook for Mechanical Engineers, Baumeister and Marks (1967).

** This table will be completed as additional bed material and baghouse/cyclone ash carbonate analysis becomes available.

TABLE 12

Material Balance

	Test Number											
	1	2	3	4	5	6	7	8	9	10	11	12
Input (lb/hr):												
Combustion Air	2226	2203	1920	1537	2372	2248	2159	2244	2327	2240	2359	2317
Feed Assist Air	146	146	146	146	146	132	132	132	132	132	132	132
Coal Feed	226	239	204	133	213	258	237	208	208	245	263	215
Sorbent Feed	0	9	6	4	6	3	9	9	15	13	16	15
Bed Material	38	12	34	7	13	0	0	0	0	0	0	0
Cyclone Ash	0	24	0	6	0	0	0	0	0	0	0	0
Total Mass In	2635	2633	2310	1833	2749	2641	2536	2593	2681	2629	2770	2679
Input (%):												
Combustion Air	84.5	83.7	83.1	83.8	86.3	85.1	85.1	86.6	86.8	85.2	85.2	86.5
Feed Assist Air	5.5	5.5	6.3	7.9	5.3	5.0	5.2	5.1	4.9	5.0	4.8	4.9
Coal Feed	8.6	9.1	8.8	7.3	7.7	9.8	9.3	8.0	7.8	9.3	9.5	8.0
Sorbent Feed	0.0	0.3	0.3	0.2	0.2	0.1	0.3	0.3	0.6	0.5	0.6	0.6
Bed Material	1.4	0.5	1.5	0.4	0.5	0.0	0.0	0.0	0.0	0.0	0.0	0.0
Cyclone Ash	0.0	0.9	0.0	0.3	0.0	0.0	0.0	0.0	0.0	0.0	0.0	0.0
Total Mass In (%)	100.0	100.0	100.0	100.0	100.0	100.0	100.0	100.0	100.0	100.0	100.0	100.0
Output (lb/hr):												
Measured Flue Gas	2250	2309	2025	1914	2787	2276	2202	2416	2364	2411	2880	2792
Flue Gas Leaks	333	302	242	-60	56	511	427	228	362	307	-56	37
Ash Out:												
Bed Material	0	21	37	19	13	13	0	10	0	21	0	11
Baghouse	12	37	15	10	24	20	21	14	21	26	23	10
Cyclone Ash	0	24	0	0	34	20	5	10	37	8	40	19
Total Mass Out	2595	2693	2319	1883	2913	2939	2655	2677	2784	2773	2888	2869
Output (lb/hr):												
Measured Flue Gas	86.7	85.7	87.3	101.7	95.7	80.2	82.9	90.2	84.9	87.0	99.7	97.3
Flue Gas Leaks	12.8	11.2	10.4	-3.2	1.9	18.0	16.1	8.5	13.0	11.1	-1.9	1.3
Ash Out:												
Bed Material	0.0	0.8	1.6	1.0	0.4	0.4	0.0	0.4	0.0	0.8	0.0	0.4
Baghouse	0.5	1.4	0.6	0.5	0.8	0.7	0.8	0.5	0.7	0.9	0.8	0.3
Cyclone Ash	0.0	0.9	0.0	0.0	1.2	0.7	0.2	0.4	1.3	0.3	1.4	0.7
Toal Mass Out (%)	100.0	100.0	100.0	100.0	100.0	100.0	100.0	100.0	100.0	100.0	100.0	100.0
Closure (%)	98.5	102.3	100.4	102.7	106.0	107.5	104.7	103.2	103.8	105.5	104.3	107.1

TABLE 13

Combustion Efficiency (Carbon Basis)

	Units	Test Number 1	2	3	4	5	6	7	8	9	10	11	12
Input													
Coal Feed Rate	lb/hr	226.0	239.4	203.8	132.5	212.7	257.5	236.6	208.2	207.6	245.4	262.6	214.8
Coal Carbon	%	64.8	62.6	62.4	62.4	63.9	63.8	64.9	62.9	63.9	64.0	64.9	63.8
Carbon Feed Rate	lb/hr	146.5	149.8	127.2	82.7	136.0	164.4	153.6	131.0	132.6	157.1	170.3	137.0
Bed Material Add Rate	lb/hr	38.0	12.0	34.0	7.0	13.0	0.0	0.0	0.0	0.0	0.0	0.0	0.0
Unburned Carbon	%	0.3	0.2	0.3	0.9	0.4	1.2	0.4	0.2	0.2	0.5	0.3	0.2
Bed Carbon Rate	lb/hr	0.1	0.0	0.1	0.1	0.1	0.0	0.0	0.0	0.0	0.0	0.0	0.0
Total		146.6	149.8	127.3	82.7	136.1	164.4	153.6	131.0	132.6	157.1	170.3	137.0
Output													
Bottom Ash Discharge Rate	lb/hr	0.0	21.0	37.0	19.0	13.0	13.0	0.0	10.0	0.0	21.0	0.0	11.0
Unburned Carbon	%	0.3	0.2	0.3	0.9	0.4	1.2	0.4	0.2	0.2	0.5	0.3	0.2
Bottom Ash Carbon Discharge Rate	lb/hr	0.0	0.0	0.1	0.2	0.0	0.2	0.0	0.0	0.0	0.1	0.0	0.0
Baghouse Discharge Rate	lb/hr	12.0	37.0	15.0	10.0	24.0	20.0	21.0	14.0	21.0	26.0	23.0	10.0
Unburned Carbon	%	10.3	8.8	5.8	4.5	9.9	17.9	9.4	4.7	6.8	12.2	17.6	7.7
Baghouse Carbon Discharge Rate	lb/hr	1.2	3.3	0.9	0.4	2.4	3.6	2.0	0.7	1.4	3.2	4.0	0.8
Total	lb/h	1.2	3.3	1.0	0.6	2.4	3.7	2.0	0.7	1.4	3.3	4.0	0.8
Combustion Efficiency	%	99.2	97.8	99.2	99.2	98.2	97.7	98.7	99.5	98.9	97.9	97.6	99.4
Process Condition													
Ave. Comb. Temp.	°F	1607	1614	1559	1351	1476	1478	1630	1615	1597	1617	1485	1470
Excess Air	%	21	22	24	54	44	17	19	41	46	21	17	46
Supervicial Gas Velocity	ft/sec	16.5	16.2	13.9	10	16.0	15.6	16.1	16.4	16.7	16.5	16.1	15.7
Gas Residence Time	sec	2.5	2.6	3.0	4.2	2.6	2.7	2.6	2.6	2.5	2.5	2.6	2.7

26

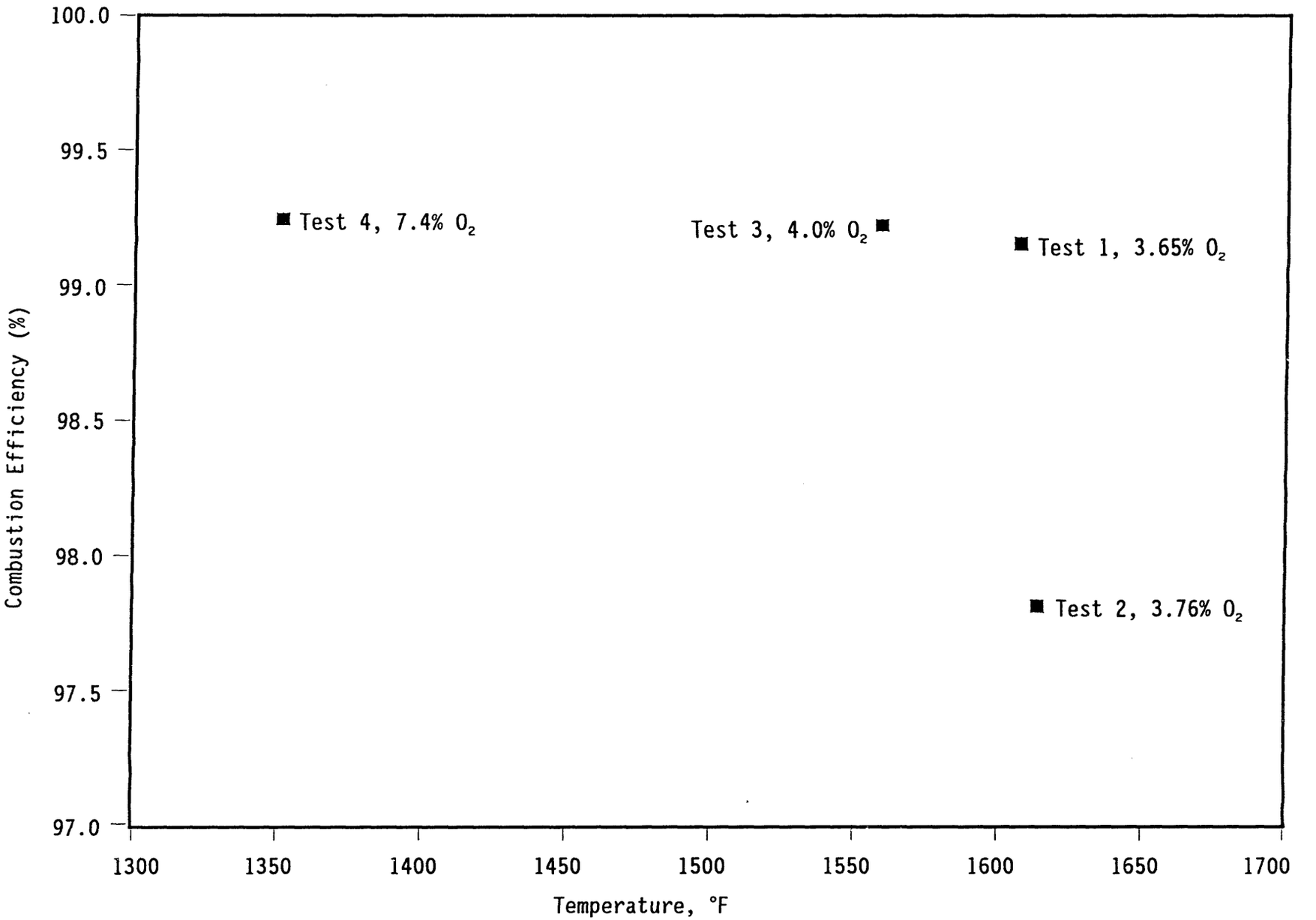

Figure 6. Combustion efficiency as a function of temperature for Tests 1-4.

solids residence times increase with the decrease in velocity. Gas residence times are listed in Table 13. A second effect was a shift in particle-size distribution. As shown in Figure 4, the size distribution in the downcomer and baghouse shifted to a smaller size for Tests 3 and 4. The increased gas residence time and the decreased cut point caused an increase in carbon burnout for Tests 3 and 4 that offset the expected temperature effects.

Figures 7 and 8 show the impacts of changing bed temperature and velocity on carbon burnout. In Figure 7 the percentage of unburned carbon in the bed material is plotted as a function of temperature. As expected, the amount of unburned carbon increases as temperature decreases. This would tend to indicate a poorer combustion efficiency at lower temperatures. The opposite trend is noted with the baghouse catch; that is, the low temperature tests have less unburned carbon in the baghouse catch than the high temperature tests. However, if one plots the unburned carbon in the baghouse catch versus velocity as in Figure 8, it can be seen that as the velocity decreases (increased residence time and decreased cut point), the amount of unburned carbon decreases. This would indicate a higher combustion efficiency as velocity decreases. The improved burnout at the lower velocities apparently offset the poorer burnout caused by the lower temperature, with the net effect being no significant difference in carbon burnout for the three load tests.

Figure 9 shows the efficiency for Tests 5 through 12 as a function of temperature. Combustion efficiency increased with increasing bed temperature and excess air level. The relatively high combustion efficiency in Test 12 may be the result of insufficient bag cleaning at the end of the test, suggested by the low baghouse discharge rate for this test. Figures 10 and 11 show the amount of unburned carbon in the bed drain and baghouse catch as a function of temperature. The percentage carbon in both the bed drain and baghouse catch is higher at the lower temperatures and excess air levels. This is different than that noted for Tests 2, 3, and 4, and reinforces the previous observations of the effect of velocity on carbon burnout and overall combustion efficiency.

6.3 Heat-Transfer Coefficient and Heat Flux

During testing, combustor heat exchange surface used for heat removal included the doors in Sections 2, 3, 4, 6, 7 and 8. Flow rates and temperatures of the cooling water used in these heat exchange surfaces was monitored to allow calculation of heat-transfer coefficients and heat flux as a function of position in the combustor. The average values of heat-transfer coefficient and heat flux for each combustor section which contains one or more heat exchange doors have been calculated for each of the twelve tests and are presented in Tables 14 and 15. Table 16 presents the average heat-transfer coefficient and heat flux for all twelve tests, along with the average pressure drop across combustor Sections 2, 4, 6 and 8. This data is also summarized in Table 6 to help facilitate comparison to test conditions. The average heat flux for the Colorado Ute Nucla Station is in the range of 28,000 to 33,000 Btu/hr-ft^2 at full load, and 20,000 to 25,000 Btu/hr-ft^2 at low load. For the twelve tests reported here, the heat flux ranged from 24,500 to 35,850 Btu/hr-ft^2 for full load tests and 18,030 Btu/hr-ft^2 at 55% load.

One of the expected trends is the decrease in heat-transfer coefficient and heat flux as a function of height (see Figures 12 and 13). The overall

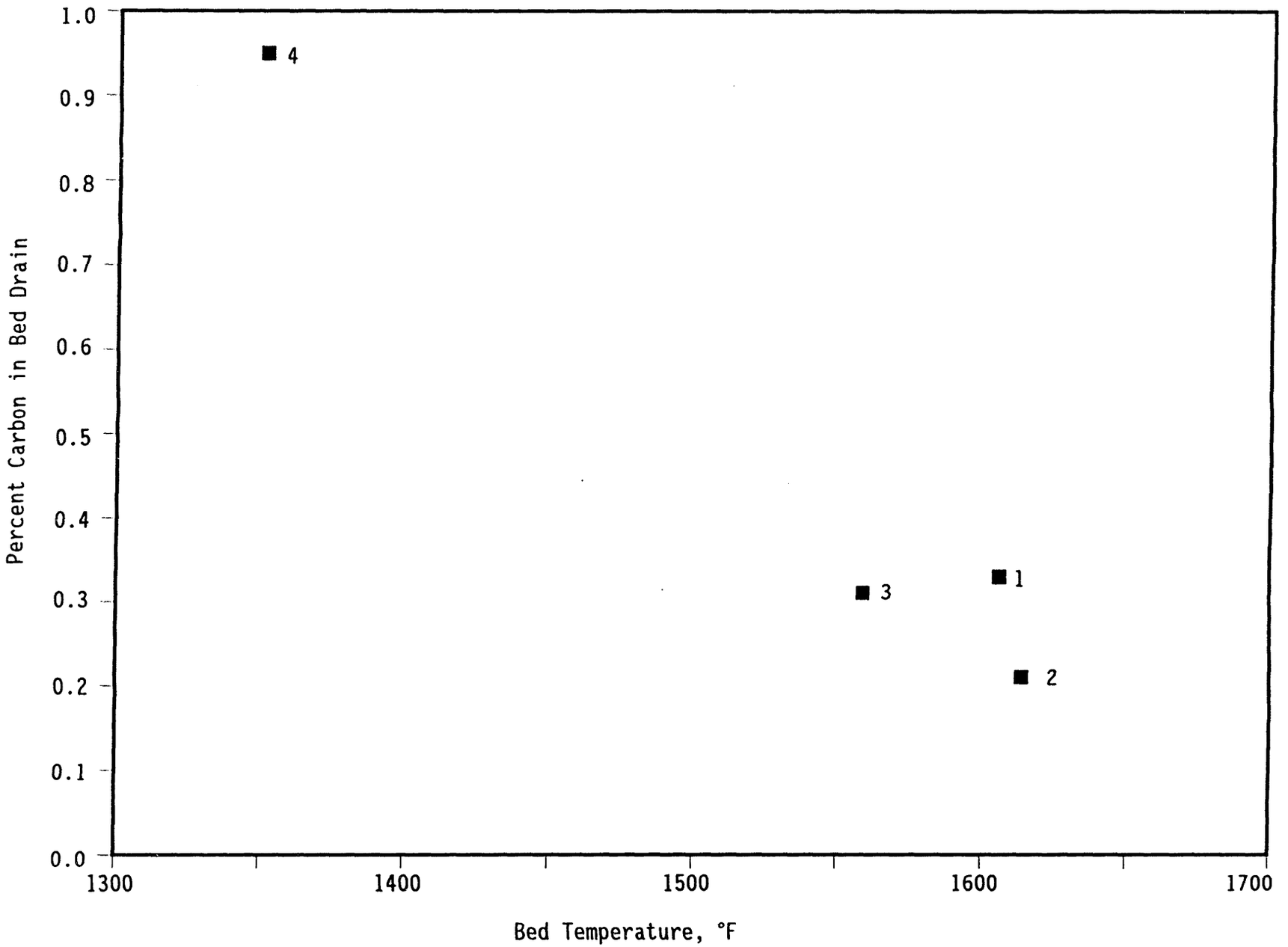

Figure 7. Percentage of unburned carbon in the combustor bed material as a function of bed temperature for Tests 1-4.

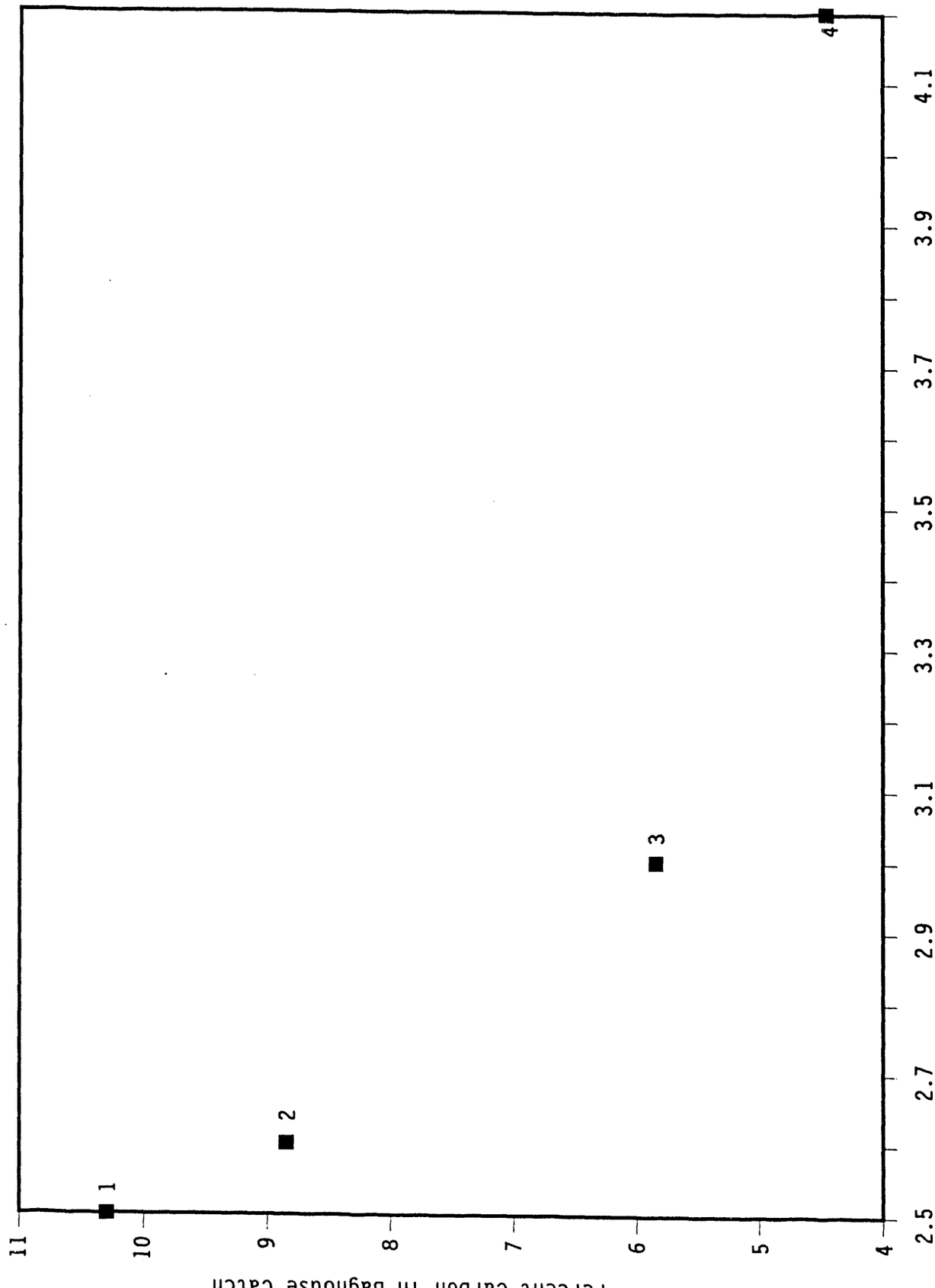

Figure 8. Percentage of unburned carbon in the fly ash as a function of gas residence time for Tests 1-4.

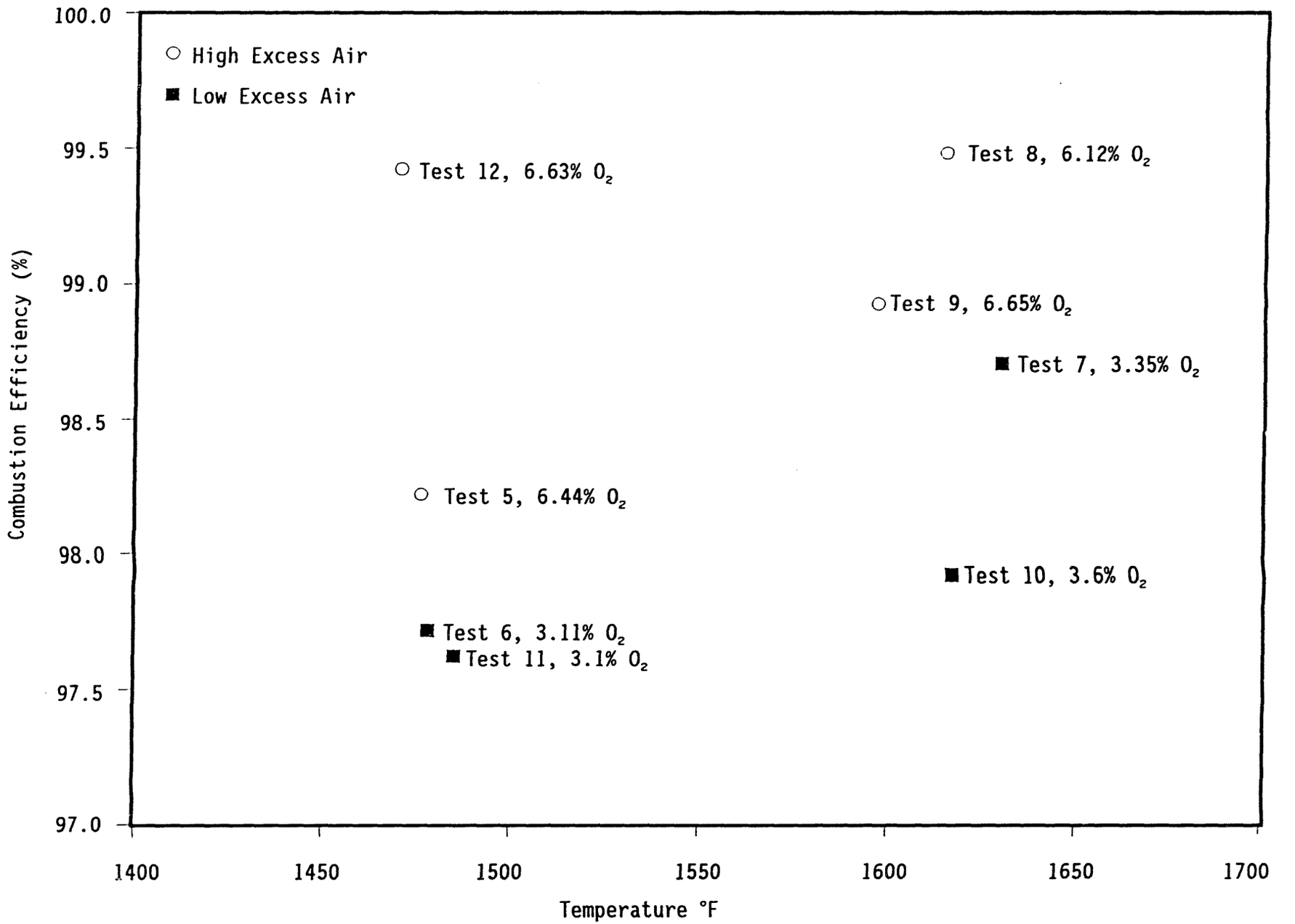

Figure 9. Combustion efficiency as a function of temperature for Tests 5-12.

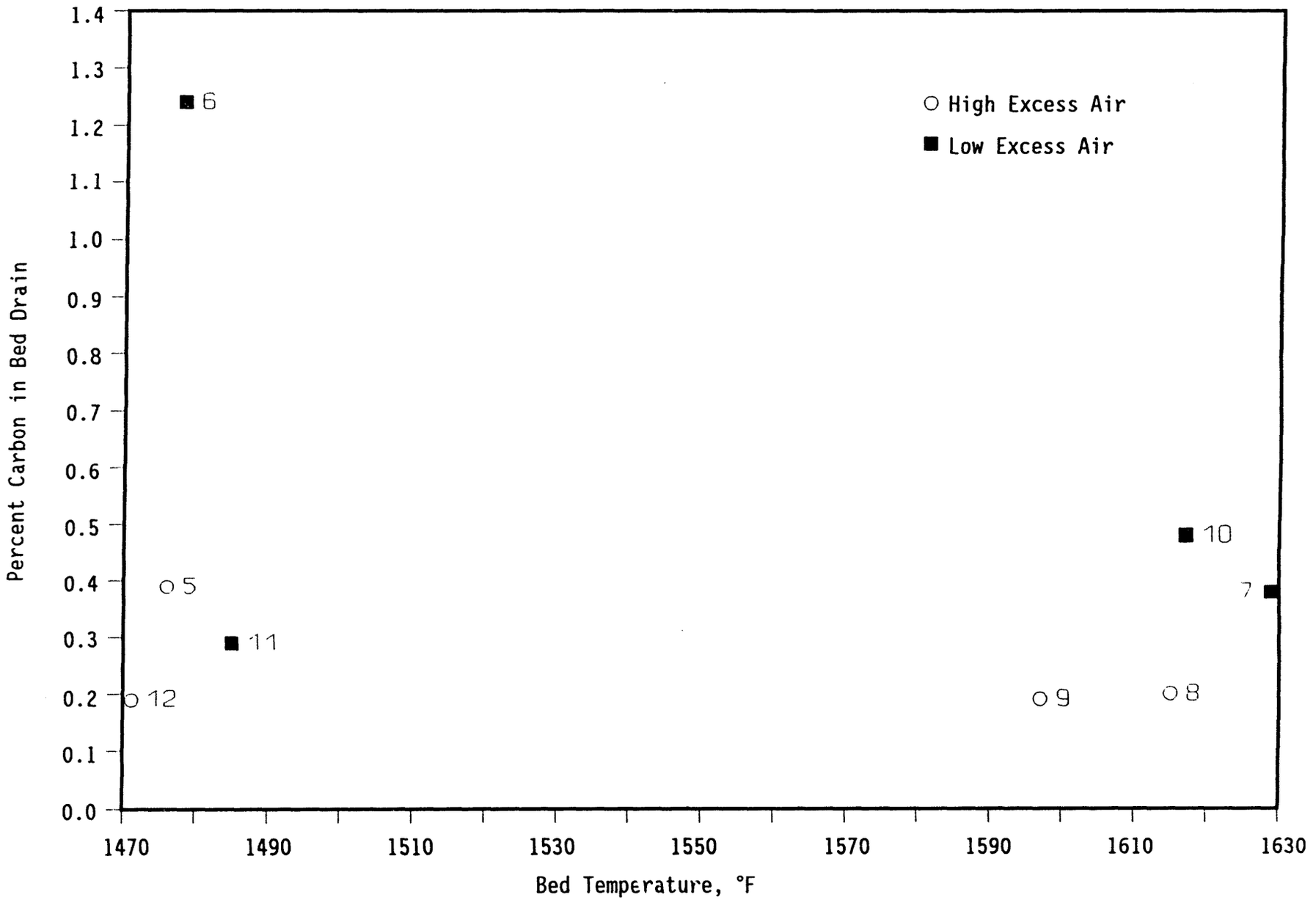

Figure 10. Percentage of carbon in bed material drain as a function of temperature for Tests 5-12.

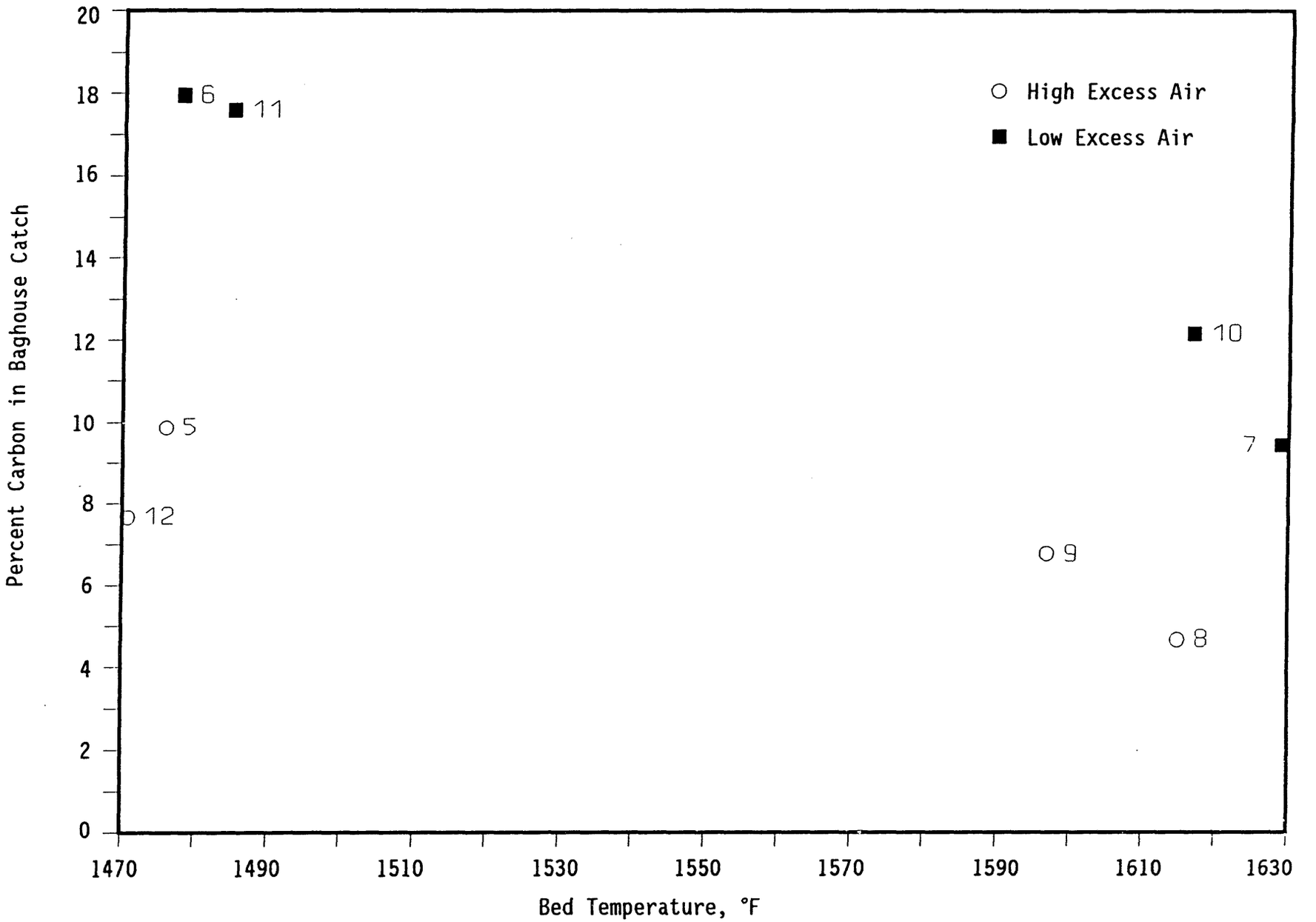

Figure 11. Percentage of carbon in the fly ash as a function of temperature for Tests 5-12.

TABLE 14

Individual Heat-Transfer Coefficient (Btu/hr-ft^2-°F)

	Test Number													
Door	1	2	3	4	5	6	7	8	9	10	11	12	Avg.	Comb. Height
2	36.9	34.6	35.1	20.4	28.9	31.9	34.0	28.6	32.0	25.8	28.9	29.5	30.6	7.5
3	26.9	27.7	22.5	16.0	23.7	21.9	25.9	22.0	26.0	23.1	24.0	22.8	23.5	12.5
4	19.1	19.0	18.8	14.2	19.8	18.6	22.6	18.5	20.9	19.2	18.7	17.4	18.9	17.5
6	19.6	20.6	18.6	14.8	18.9	19.0	20.9	18.9	21.1	19.7	19.8	16.5	19.0	27.5
7	17.8	19.3	17.3	13.7	19.8	19.6	22.8	20.0	22.1	20.0	19.7	17.9	19.2	32.5
8	19.1	11.1	17.7	14.7	20.9	17.9	21.3	19.2	21.9	17.0	22.2	18.0	18.4	37.5
H_o*	23.7	21.0	22.7	14.4	20.5	22.0	24.1	20.8	23.1	17.3	19.8	18.4	20.7	--

* H_o = Overall heat-transfer coefficient for the combustor.

TABLE 15

Individual Heat Flux (Btu/hr-ft^2)

	Test Number													
Door	1	2	3	4	5	6	7	8	9	10	11	12	Avg.	Comb. Height
2	53,650	50,890	49,250	25,029	38,460	41,970	49,950	42,130	46,300	38,310	38,490	38,820	42,771	7.5
3	39,570	40,490	32,740	20,770	32,260	30,180	38,850	33,180	38,240	34,700	32,550	30,530	33,672	12.5
4	28,400	28,330	26,820	17,980	26,480	25,410	33,560	27,540	30,340	28,520	25,530	23,480	26,866	17.5
6	28,800	30,450	26,500	18,540	25,410	26,236	31,366	28,090	30,790	29,000	26,540	22,010	26,978	27.5
7	26,110	28,380	24,400	17,060	26,270	26,310	33,820	29,330	31,570	29,260	26,270	23,640	26,868	32.5
8	27,760	16,390	24,980	18,118	27,200	25,090	32,220	28,810	31,870	14,480	29,720	24,300	25,078	37.5
Flux*	34,690	30,900	32,140	18,030	27,400	29,680	35,850	30,930	33,570	25,710	26,720	24,580	29,183	--

* Flux = Overall heat flux for the combustor.

TABLE 16

Average Heat-Transfer Coefficient, Heat Flux, and Bed Density

Section	dP (in.H_2O col.)	H_o (Btu/hr-ft^2-°F)	Flux (Btu/hr-ft^2)	Bed Density (lbs/ft^3)
2	38.6	30.6	38,900	40.32
4	3.2	18.9	24,300	1.67
6	1.5	19.0	24,400	0.78
8	0.2	18.4	22,400	0.10
1-8	44.2	20.7	26,400	

mass density of bed material in the combustor decreases with combustor height. The decrease in pressure drop with combustor height provides a measure of this decrease in mass density. At the bottom of the combustor, below the secondary air port, there is a relatively dense bed, and high heat fluxes and heat-transfer coefficients similar to those of bubbling beds are present. In the higher velocity region above the secondary air ports, the bed is less dense. This transition from a dense to dilute bed is common for all CFBCs, irrespective of the type and location of secondary air ports, or if secondary air is used at all. The transition point from dense to dilute bed will change somewhat, however, depending upon the design of the unit. The heat flux and heat-transfer coefficients are expected to follow a similar trend for all units.

The impact of operating conditions on heat transfer can be seen by comparing values from test to test. As load is decreased, the velocity also decreases, causing a decrease in solids recirculation rate and a decrease in the density within the upper regions of the bed. As expected, both the combustor heat flux and heat-transfer coefficients decrease, as shown graphically in Figures 12 and 13, respectively, for full and 55% load situations. Another expected trend is the impact of operating temperature on heat flux. As shown in Figure 14, the heat flux increases as the average-bed temperature (driving force for heat transfer) increases. The heat-transfer coefficient did not vary with temperature over this range of test conditions.

Other conditions appear to have smaller impacts on the heat flux and heat-transfer coefficients. It should be noted that the differences measured were within the standard deviation of the averages and, therefore, may not be statistically significant. As other test runs are completed, similar data will be compared to determine if the following effects are real or due to random data scatter. As the Ca/S was increased from an average of 2.1 to 4.0, the heat flux and heat-transfer coefficient decreased. It would be expected that as the limestone feed rate increased, the amount of fine solids would increase, thereby increasing the solids recirculation rate, and increase the heat flux and heat-transfer coefficient. Therefore, this effect may be due to random error in measurement, but will be investigated in future testing. The other effect noted was a slight increase in the heat flux and heat-transfer coefficient as the primary-to-total air split was increased from an average of 48% to 67%. This could be a real effect, resulting from more solids in the primary zone being carried into the upper reaches of the combustor as the amount of primary air increased. Higher velocities exist in the primary zone at higher primary air ratios.

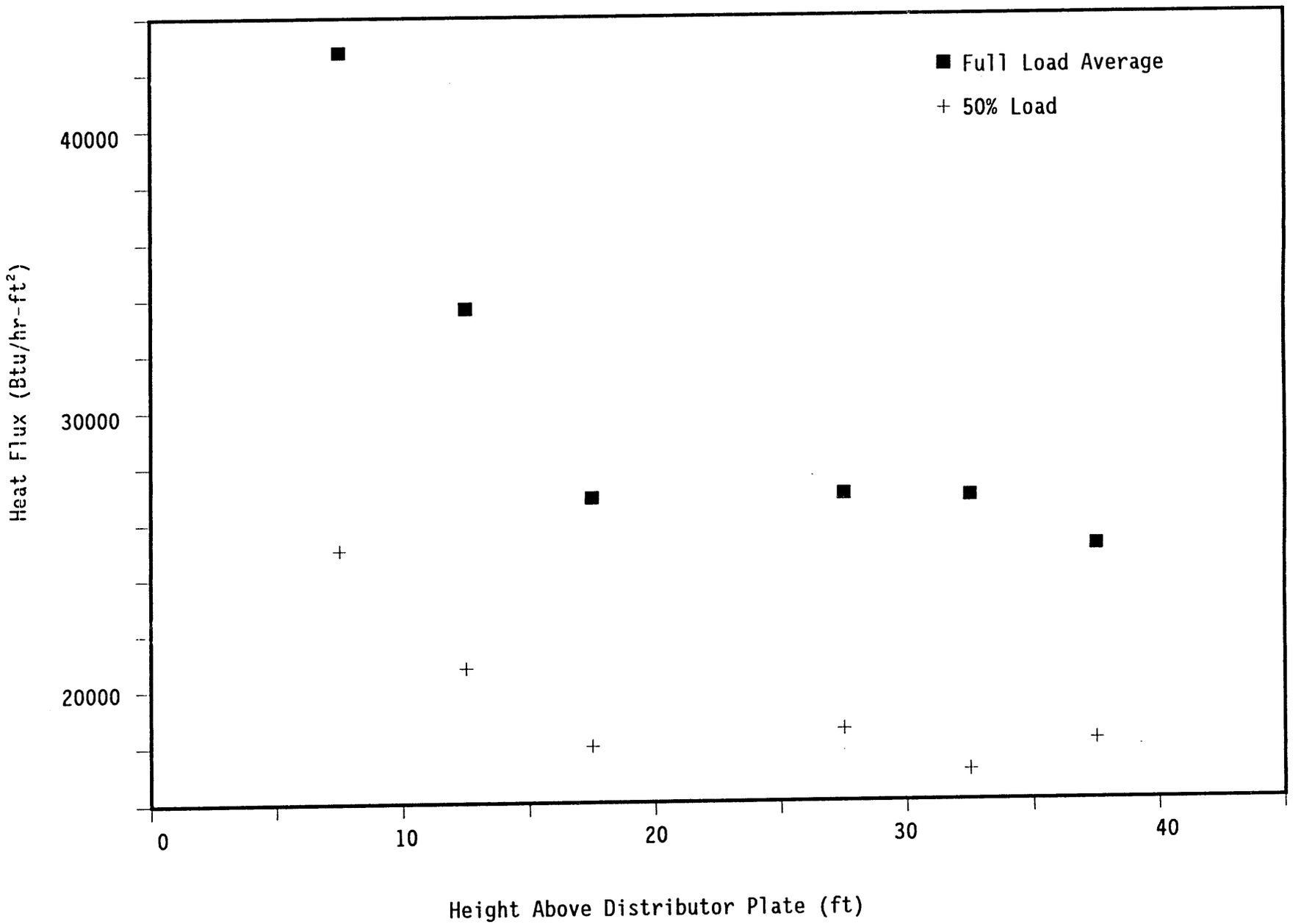

Figure 12. Heat flux as a function of combustor height.

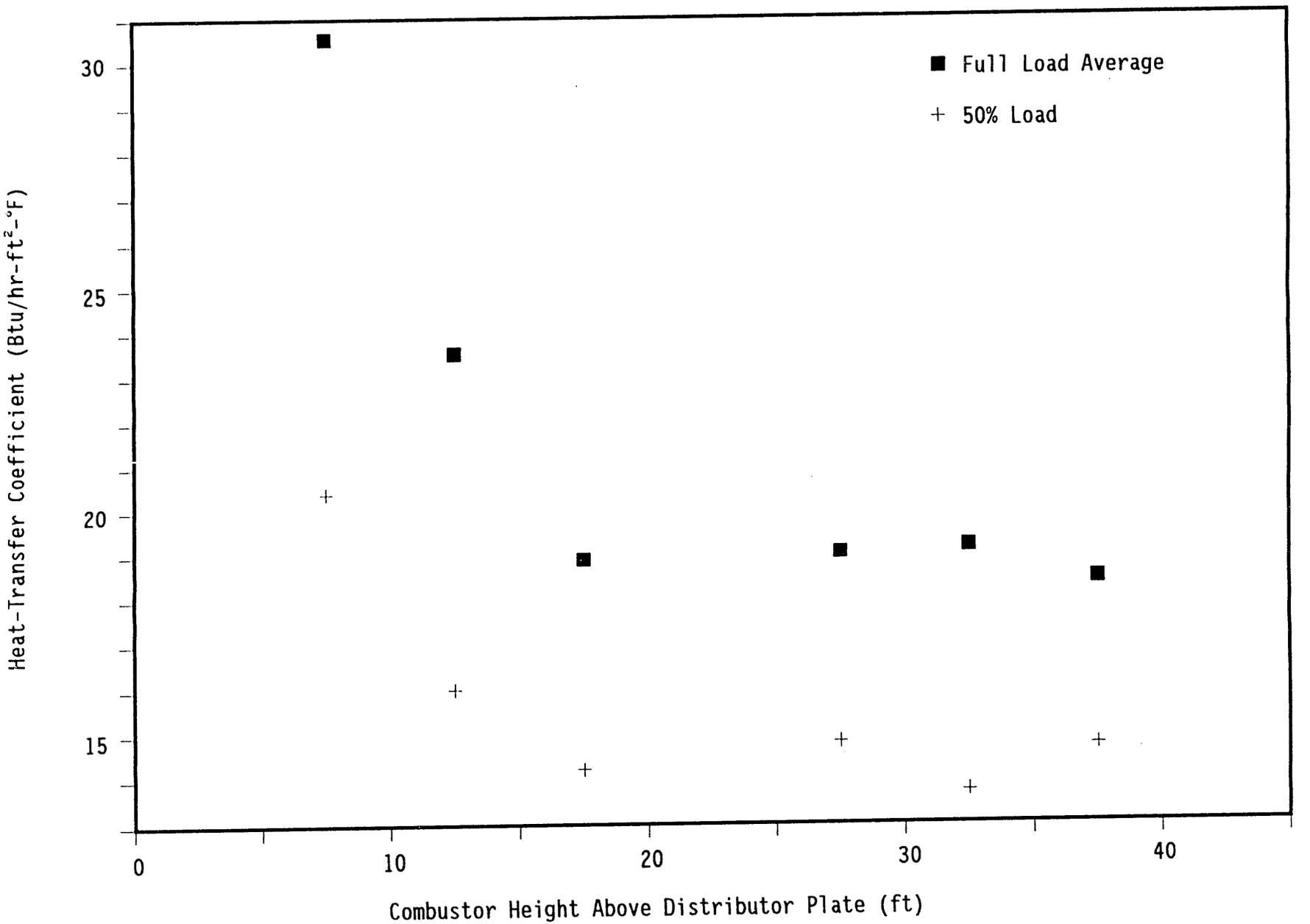

Figure 13. Heat-transfer coefficient as a function of combustor height.

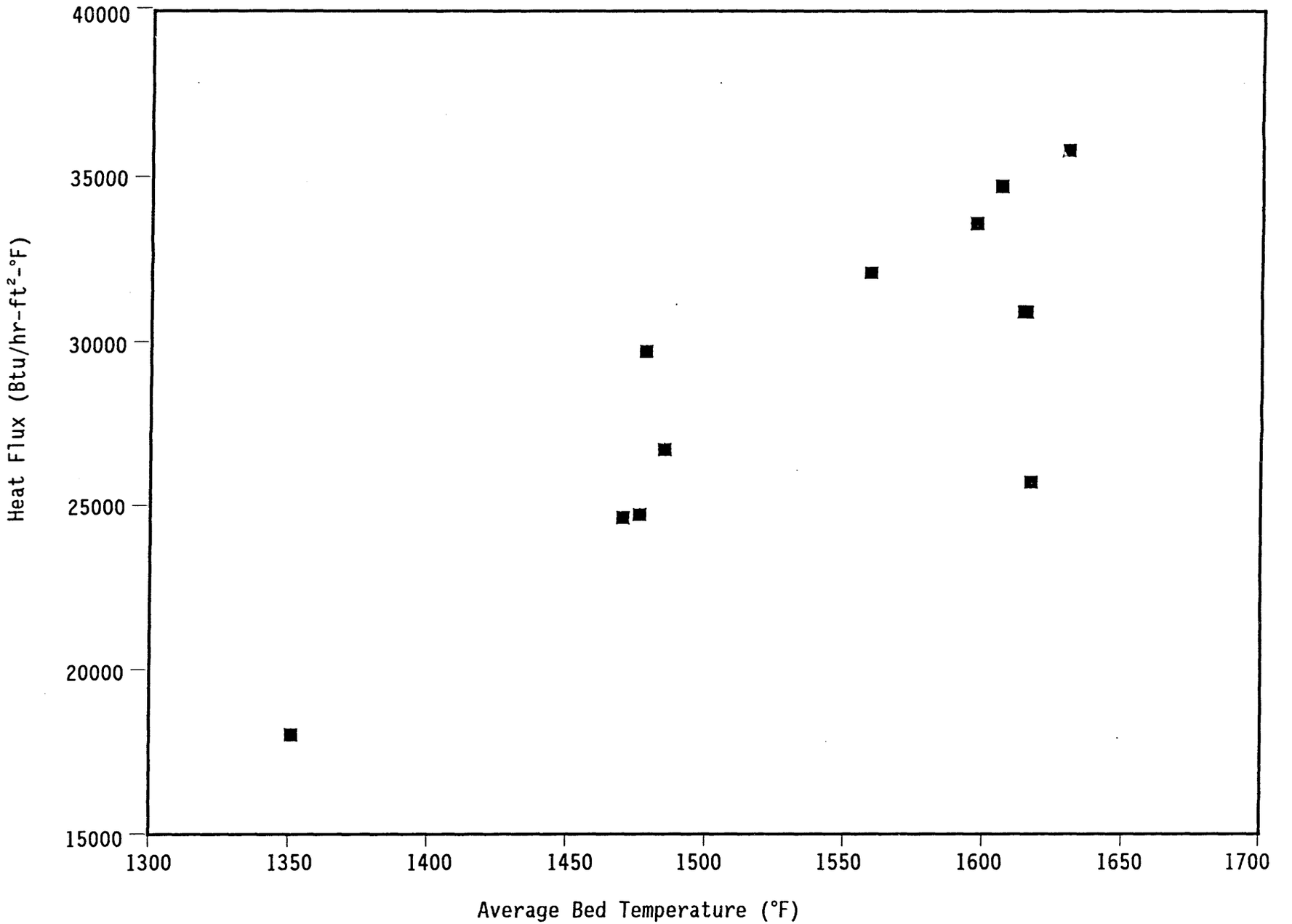

Figure 14. Heat-transfer coefficient as a function of average bed temperature.

7.0 ENVIRONMENTAL PERFORMANCE

The flue gas emissions for each test period are shown in Table 17. Figure 15 shows the average emission levels at different load conditions. Load was reduced by setting the coal feed to 85% or 55% of the full-load feed rate. Heat exchange surfaces in the combustor and external heat exchanger remained constant, so that the temperature in the partial-load conditions dropped accordingly. Excess air was high (54%) during the 55% load test. Furthermore, superficial gas velocity in the combustor decreased, as a result of lower air flow rates and lower combustor temperatures. The N_2O emissions were highest at the 55% load condition, as expected; the formation of N_2O is inversely proportional to temperature and directly proportional to excess air. NO_x showed the opposite trend, but to a lesser degree. The SO_2 emissions were lowest during the 85% load test, when the average temperature was 1559°F. Calcium utilization was greatest at this temperature, as shown in Table 17.

7.1 SO_2 Emissions

Figure 16 shows SO_2 retention as a function of alkali-to-sulfur (A/S) ratio for full load Tests 1, 2, and 10, presented as both alkali in the limestone alone as well as total alkali content. These three tests were performed at the same bed temperature, excess air level, and primary air split. SO_2 retention increased with greater alkali addition. In order to achieve 70% retention, an added A/S ratio of about 2.5 would be required at these operating conditions. The average bed temperature of 1625°F used for these tests is above the optimal temperature window for sulfur capture (1500° to 1550°F). Therefore, lower add rates of sorbent would be needed to meet 70% retention within the optimal sulfur capture window. About 7% to 10% of the sulfur retention was due to the alkali inherent to the coal.

Figure 17 presents the sulfur retention as a function of total alkali-to-sulfur ratio for all of the tests, with the exception of the 55% load test. The increase in sulfur retention with increasing A/S ratio is evident. Also important is the effect of temperature on sulfur retention. At a given A/S ratio, the lowest retention was obtained at 1613°, higher at 1417°, and the highest at 1559°F. This trend is as expected, as the optimal sulfur capture is usually achieved in the range of 1500° to 1550°F. For future testing, additional temperature tests would be desirable to identify the optimal temperature and maximum sulfur retention for the test coal. The impact of alkali-to-sulfur ratio and temperature on SO_2 emissions are shown in Figure 18.

Figure 19 shows that the calcium utilization was greatest at a low calcium-to-sulfur ratio, decreased as Ca/S ratio was increased to about 2.5, then leveled off at a calcium utilization of about 25% with increasing Ca/S. This is the normal trend for any calcium-based sulfur control system. At low Ca/S ratios, only a portion of the sulfur is captured, so there is a relatively high driving force. As the Ca/S ratio increases, more sulfur is captured and less is available in the gas stream for capture, thereby reducing the sulfur concentration driving force.

7.2 NO_x Emissions

NO_x emissions ranged from 31 to 216 ppm (0.04 to 0.35 lb/MM Btu), as measured. NO_x emissions are dependent upon several factors, including

TABLE 17

Emissions Data

	Test Number											
	1	2	3	4	5	6	7	8	9	10	11	12
O_2, %	3.65	3.76	4.0	7.4	6.44	3.11	3.35	6.12	6.65	3.6	3.1	6.63
CO Content, ppm	50.0	53.0	65.0	145.0	75.0	120.0	50.0	50.0	45.0	45.0	95.0	70.0
CO Content, ppm*	51.9	55.3	68.8	191.9	92.7	120.7	51.0	60.5	56.4	46.6	95.5	87.7
CO Emission, lb/MM Btu	0.041	0.044	0.053	0.148	0.074	0.100	0.041	0.047	0.044	0.037	0.078	0.070
CO_2 Content, %	15.9	15.7	16.2	12.8	13.3	15.7	16.0	13.8	13.5	15.9	16.0	13.0
CO_2 Content, %*	16.5	16.4	17.1	17.0	16.5	15.8	16.3	16.7	16.9	16.5	16.1	16.3
NO_x Content, ppm	137	150	110	39	75	31	113	161	216	139	55	123
NO_x Content, ppm*	143	158	117	51	93	32	115	194	272	145	56	154
NO_x Emission, lb/MM Btu	0.19	0.21	0.15	0.07	0.12	0.04	0.15	0.25	0.35	0.19	0.08	0.21
N_2O Content, ppm	145	136	180	325	251	217	112	120	135	120	222	232
N_2O Content, ppm*	150	143	191	431	310	219	115	146	169	124	223	291
N_2O Emission, lb/MM Btu	0.19	0.18	0.23	0.52	0.39	0.29	0.15	0.18	0.21	0.16	0.29	0.37
SO_2 Content, ppm	511	173	133	139	136	210	223	162	21	91	45	35
SO_2 Content, ppm*	530	179	123	184	168	211	227	196	26	94	41	34
SO_2 Emission, lb/MM Btu	0.96	0.33	0.25	0.32	0.31	0.40	0.42	0.35	0.05	0.17	0.08	0.08
SO_2 Retention (meas.), %	0.7	66.0	74.3	66.2	68.1	58.5	56.6	63.3	95.1	82.3	91.3	91.5
SO_2 Retention (calc), %**	0.7	67.2	74.6	66.0	67.7	57.1	55.4	67.7	95.2	82.9	91.5	92.2
Ca/S Ratio (ls only)	0.0	2.6	2.2	2.4	2.2	1.0	2.6	2.6	4.9	3.4	4.0	4.4
Ca/S Ratio (total)	0.3	3.0	2.6	2.8	2.5	1.4	3.0	2.8	5.2	4.0	4.3	4.7
Adj. Ca/S Ratio (ls only)	0.0	2.2	1.8	2.0	1.8	0.8	2.2	2.2	4.1	2.9	3.5	3.8
Adj. Ca/S Ratio (total)	0.3	2.5	2.1	2.4	2.1	1.1	2.5	2.5	4.4	3.5	3.7	4.1
Ca Utiliz. (ls only)	0.0	25.5	34.1	27.1	31.5	58.2	21.1	26.5	19.5	24.6	22.8	21.0
Ca Utiliz. (total)	2.2	22.1	28.9	23.3	27.0	41.1	18.4	23.9	18.4	20.8	21.4	19.5
Avg. Comb. Temp., °F	1607	1614	1559	1351	1476	1478	1630	1615	1597	1617	1485	1470
C in Coal, %	60.4	57.6	57.6	57.7	59.6	58.9	59.9	58.2	58.7	59.0	59.7	58.7
CaO in LS, %	52.0	52.0	52.0	52.0	52.0	52.0	52.0	52.0	52.0	52.0	52.0	52.0
CaO in Coal Ash, %	1.5	1.6	1.5	1.4	1.4	1.5	1.6	1.2	1.2	2.7	1.2	1.6
S in Coal, %	0.43	0.43	0.41	0.41	0.41	0.40	0.41	0.50	0.44	0.46	0.46	0.48
Adj. S. in Coal	0.52	0.52	0.50	0.49	0.50	0.49	0.50	0.57	0.52	0.53	0.53	0.55
% Ash in Coal, dec %	0.17	0.19	0.19	0.20	0.18	0.19	0.17	0.20	0.19	0.19	0.18	0.18
Coal Feed Rate, lb/hr	226	239	204	133	213	258	237	208	208	245	263	215
Sorbent Feed Rate, lb/hr	0.0	9.1	6.2	4.5	6.3	3.4	8.6	9.0	15.1	12.8	16.4	15.3
Moisture in Coal, %	6.8	7.9	7.8	7.5	6.8	7.8	7.8	7.5	8.2	7.9	7.9	7.9
Moisture in FG, %	5.5	5.4	5.3	3.7	4.1	5.9	5.7	4.4	4.4	5.3	4.6	4.0
Theor. FG Flow Rate, scfm	556	562	488	399	612	600	566	569	587	585	608	609
Meas. FG Flow Rate, scfm	481	497	436	412	600	490	474	520	509	519	620	601
Moisture-Free Coal Carbon, %	64.8	62.6	62.4	62.4	63.9	63.8	64.9	62.9	63.9	64.0	64.9	63.8
Moisture-Free Coal Sulfur, %	0.56	0.57	0.57	0.56	0.56	0.57	0.57	0.56	0.57	0.57	0.57	0.57
Adj. Moist-Free Coal S %	0.56	0.56	0.54	0.53	0.54	0.53	0.54	0.61	0.56	0.57	0.57	0.59

* Corrected to 3% O_2

** Moisture-free coal carbon and sulfur values used in the sulfur retention calculation.

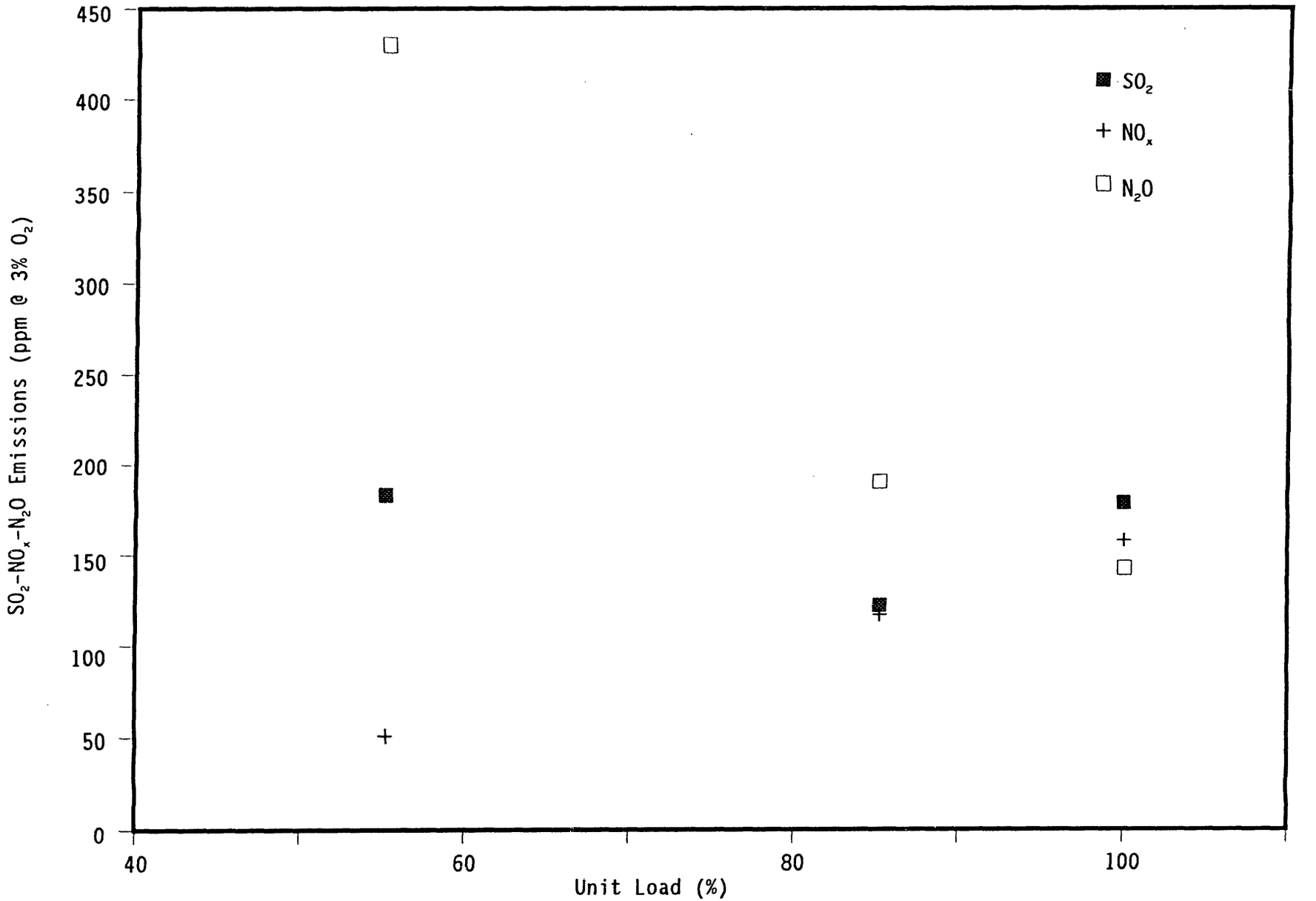

Figure 15. Flue gas emissions as functions of load.

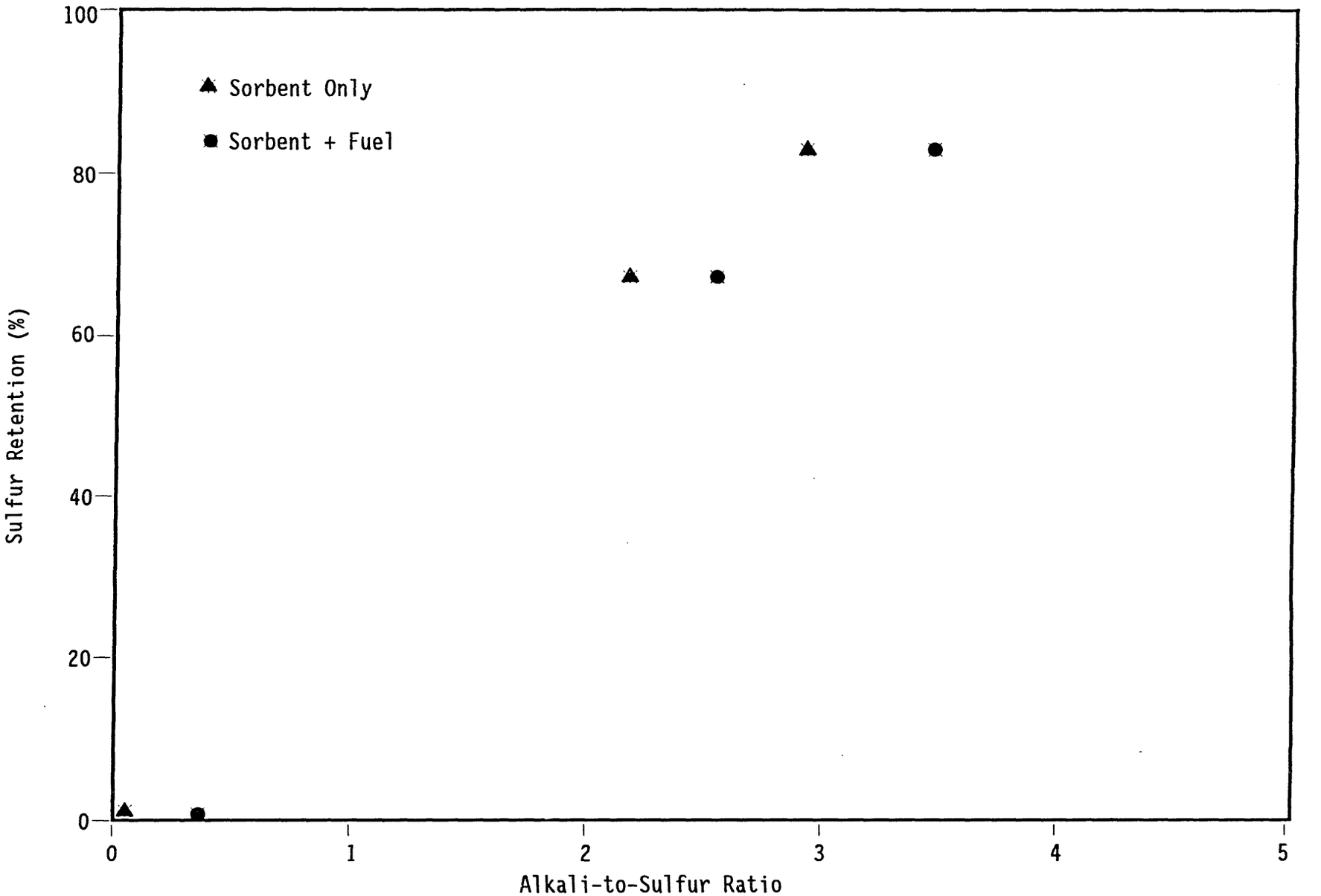

Figure 16. SO_2 retention as a function of alkali-to-sulfur ratio for Tests 1, 2, and 10.

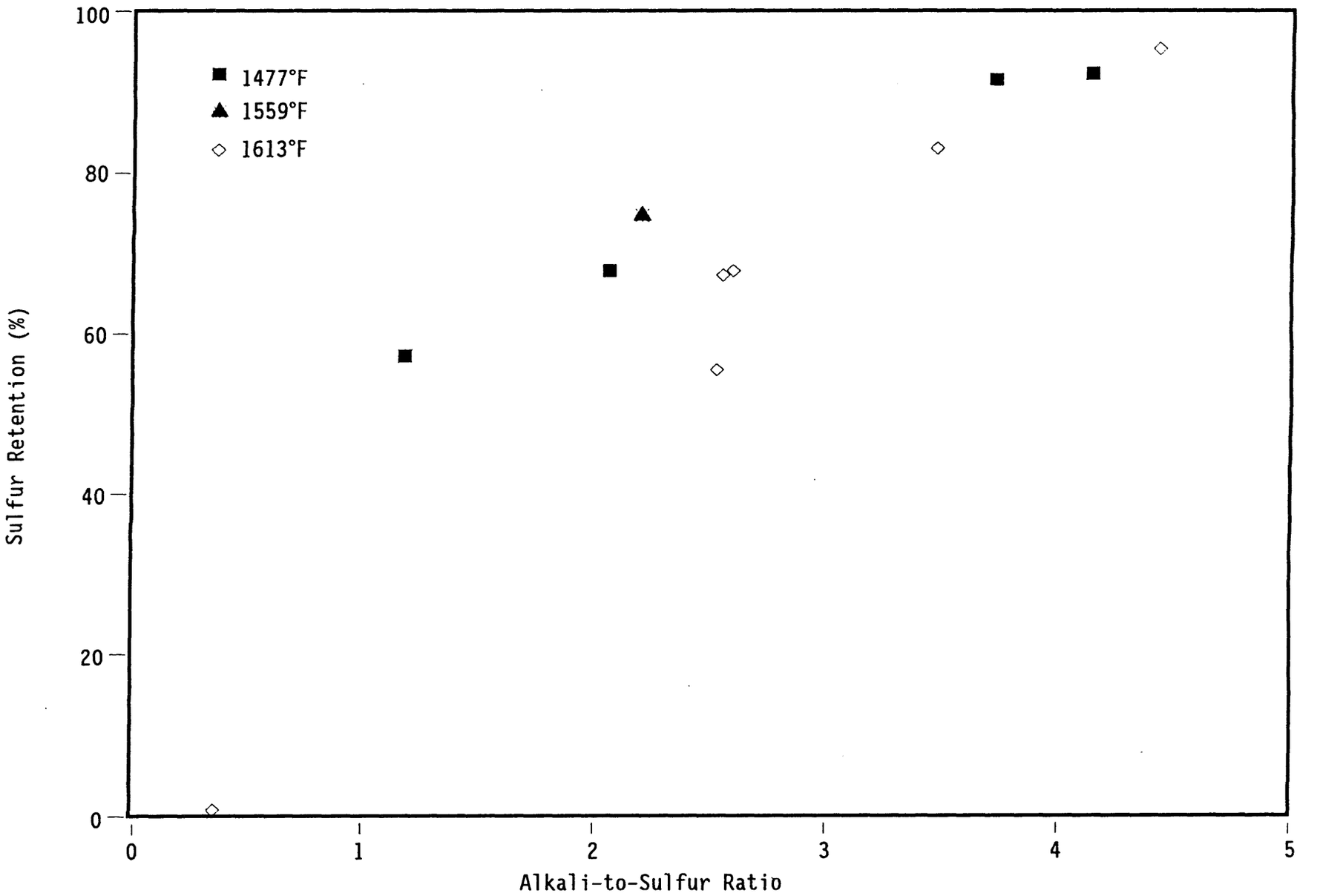

Figure 17. The effects of total alkali-to-sulfur ratio and temperature on SO_2 retention.

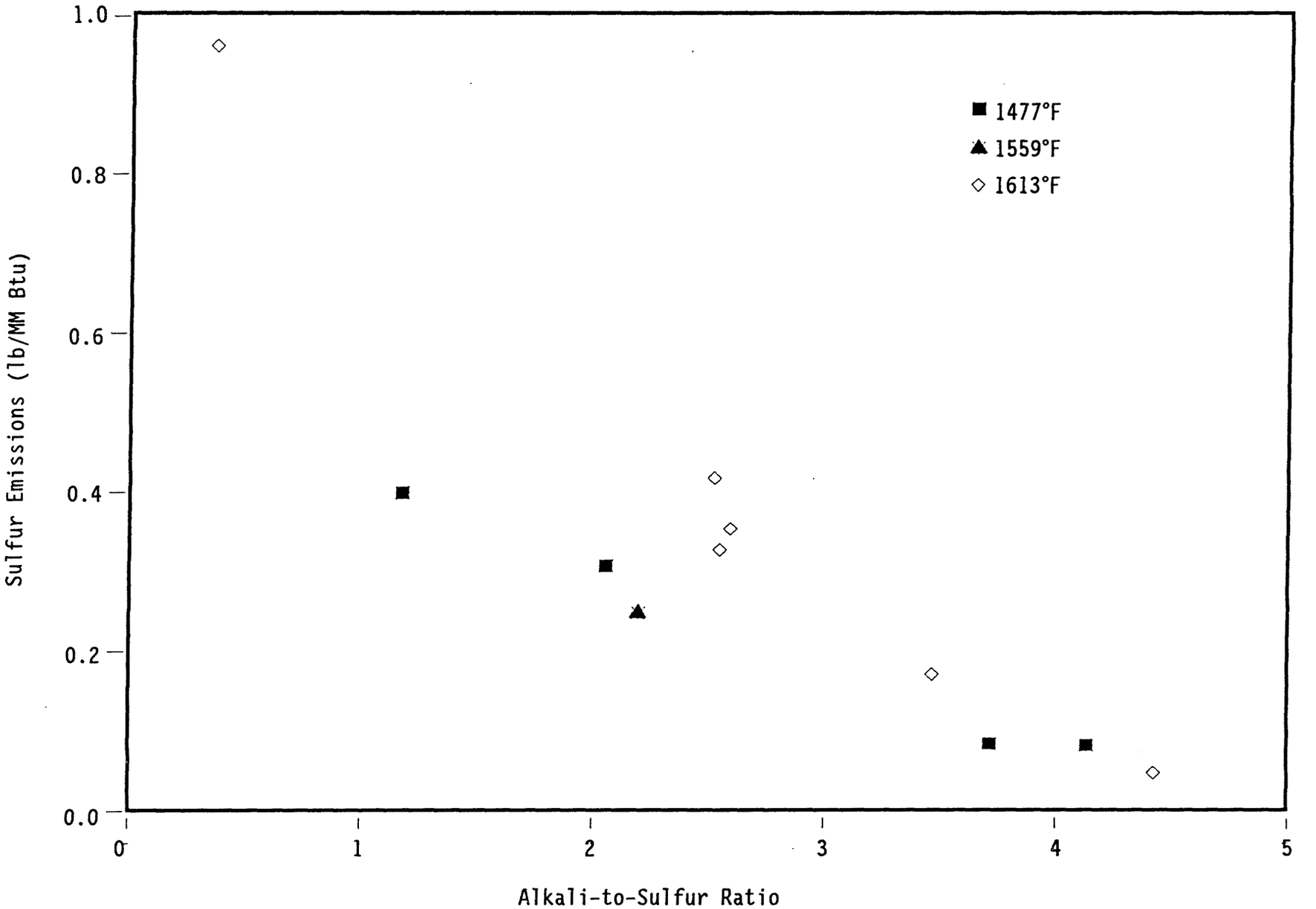

Figure 18. The effects of total alkali-to-sulfur ratio and temperature on SO_2 emissions.

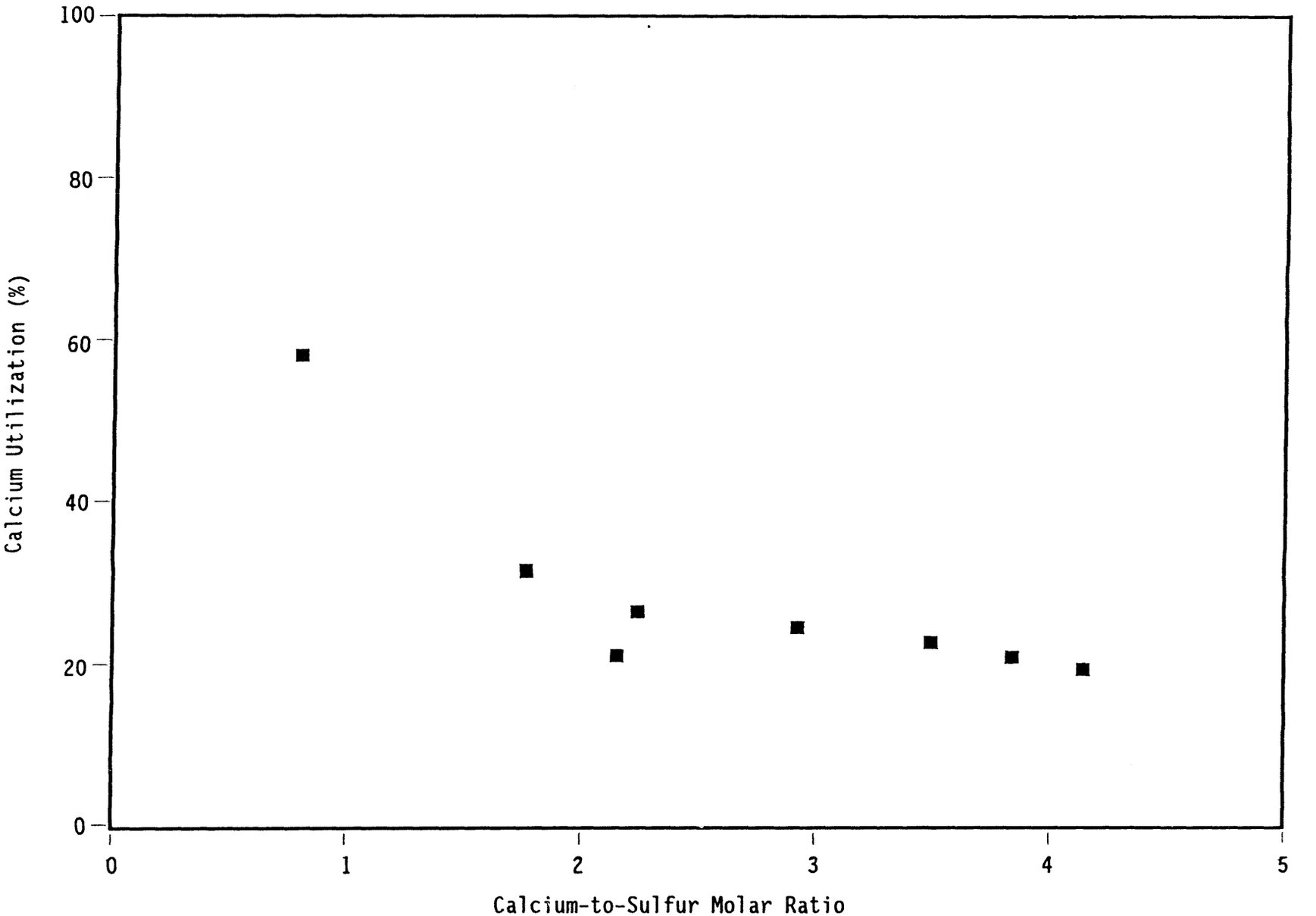

Figure 19. Calcium utilization as a function of added calcium-to-sulfur ratio.

temperature, oxygen content, and alkali-to-sulfur ratio. Figure 20 shows some of these effects. At low temperature and low excess air (oxygen content), the NO_x levels were predictably low. NO_x increased with an increase in temperature and/or an increase in excess air. High temperature and high excess air produced the greatest NO_x emissions. In each temperature-excess air system, more NO_x was released at the higher calcium-to-sulfur ratio. These trends are similar to those produced in other FBC systems, in terms of both bubbling and circulating designs.

7.3 N_2O Emissions

N_2O emissions were greatest at low temperature, as shown in Figure 21. The effect of excess air on N_2O emissions is negligible at high temperature (greater than 1500°F); however, at lower temperature, the N_2O emissions are significantly greater at the higher level of excess air. This trend is evident at a temperature of approximately 1475°F in Figure 19, although the test matrix did not include a low temperature (1350°F)-low excess air (20%) operating condition to verify the trend. Measured values of N_2O ranged from 29 to 325 ppm (0.04 to 0.52 lb/MM Btu). Currently, there are no federal standards controlling N_2O emissions.

7.4 CO Emissions

Table 17 indicated that the CO emissions from all tests were relatively low (45 to 145 ppm). Figure 22 is a graph of the CO concentration corrected to 3% O_2 as a function of temperature which shows that the CO emissions were greatest at low temperatures, as expected.

8.0 COMPARISON TO FULL SCALE

8.1 Heat Flux

The heat flux and heat-transfer coefficients are influenced primarily by bed hydrodynamics. The solids recirculation rate, bed particle size and type, velocity, and temperature all influence heat transfer in the CFBC. These parameters can be, and were, duplicated fairly well in the EERC pilot plant, as compared to the commercial plant. Therefore, one may expect the bed hydrodynamics to be similar between the pilot- and full-scale units. However, the impacts of a higher degree of wall effects for the smaller pilot-scale unit and more pronounced circulation patterns for larger units is difficult to assess. The relative degree of these differences and their importance in process comparison between pilot and full scale is difficult to assess, and further research is needed to quantify differences between pilot and full scale.

A comparison of the heat flux data from the pilot- and full-scale plant indicates that a reasonable assessment of heat flux can be measured in the pilot-scale unit. The measured heat flux from the pilot-scale testing ranged from 24,500 to 35,850 Btu/hr-ft^2 at full load conditions, with the variability due to changes in operating conditions including bed temperature and primary-to-total air split. At 55% load, the heat flux was only 18,030 Btu/hr-ft^2. The measured heat flux from the Colorado Ute Nucla Station ranged from 28,000 to 33,000 Btu/hr-ft^2 at full load and 20,000 to 25,000 Btu/hr-ft^2 at part load.

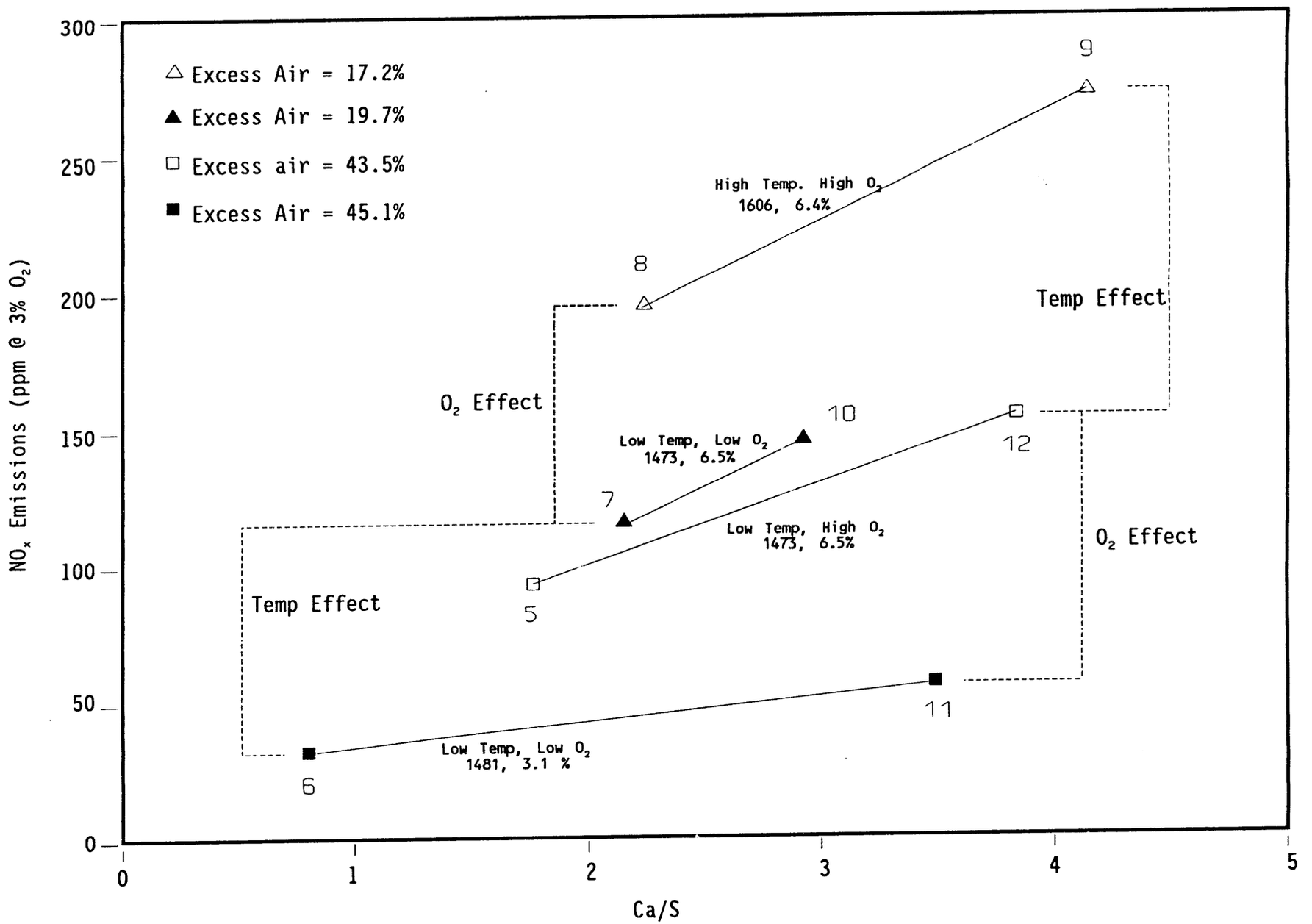

Figure 20. The effects of calcium-to-sulfur ratio, excess air, and temperature on NO_x emissions.

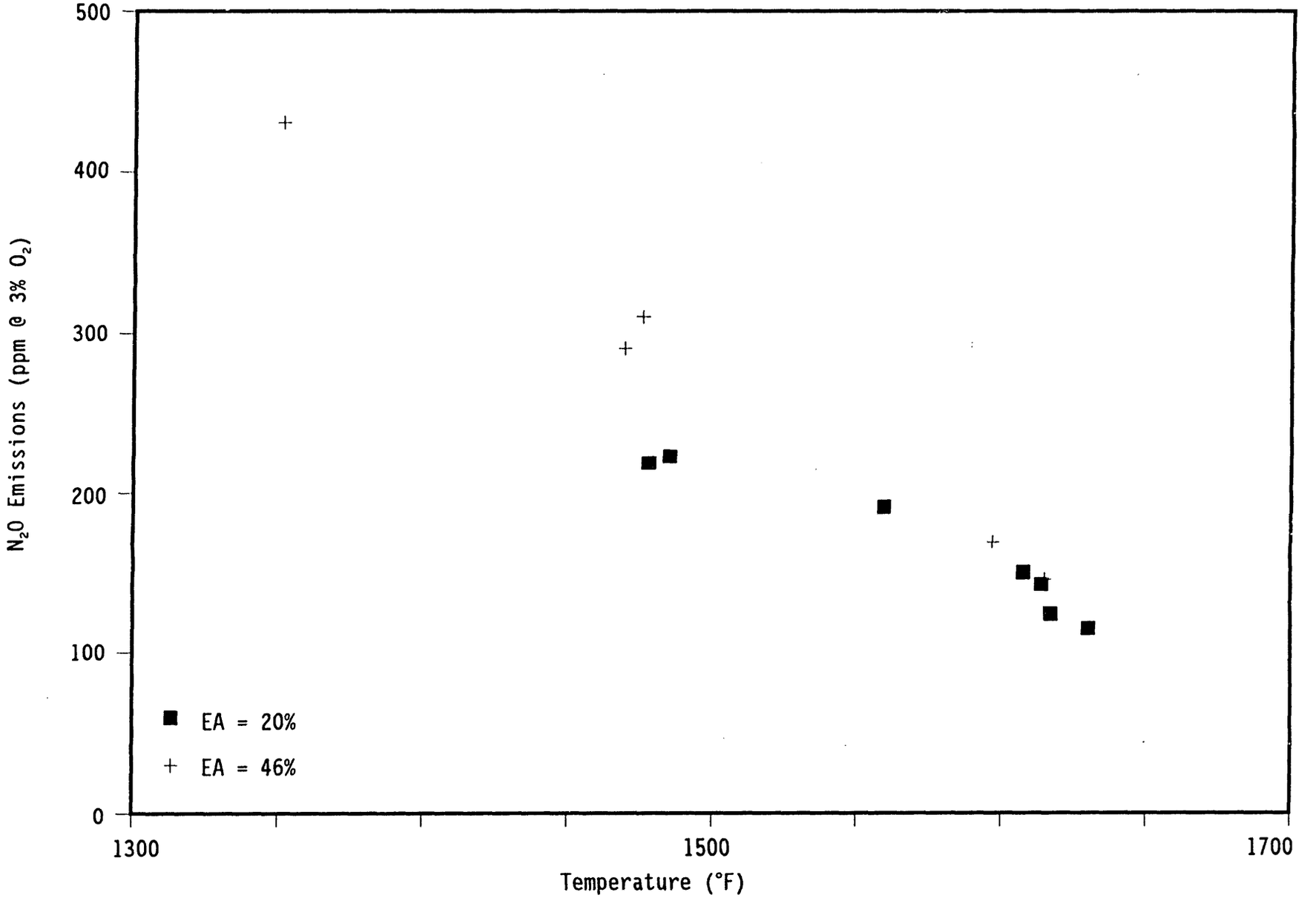

Figure 21. The effects of temperature and excess air on N_2O emissions.

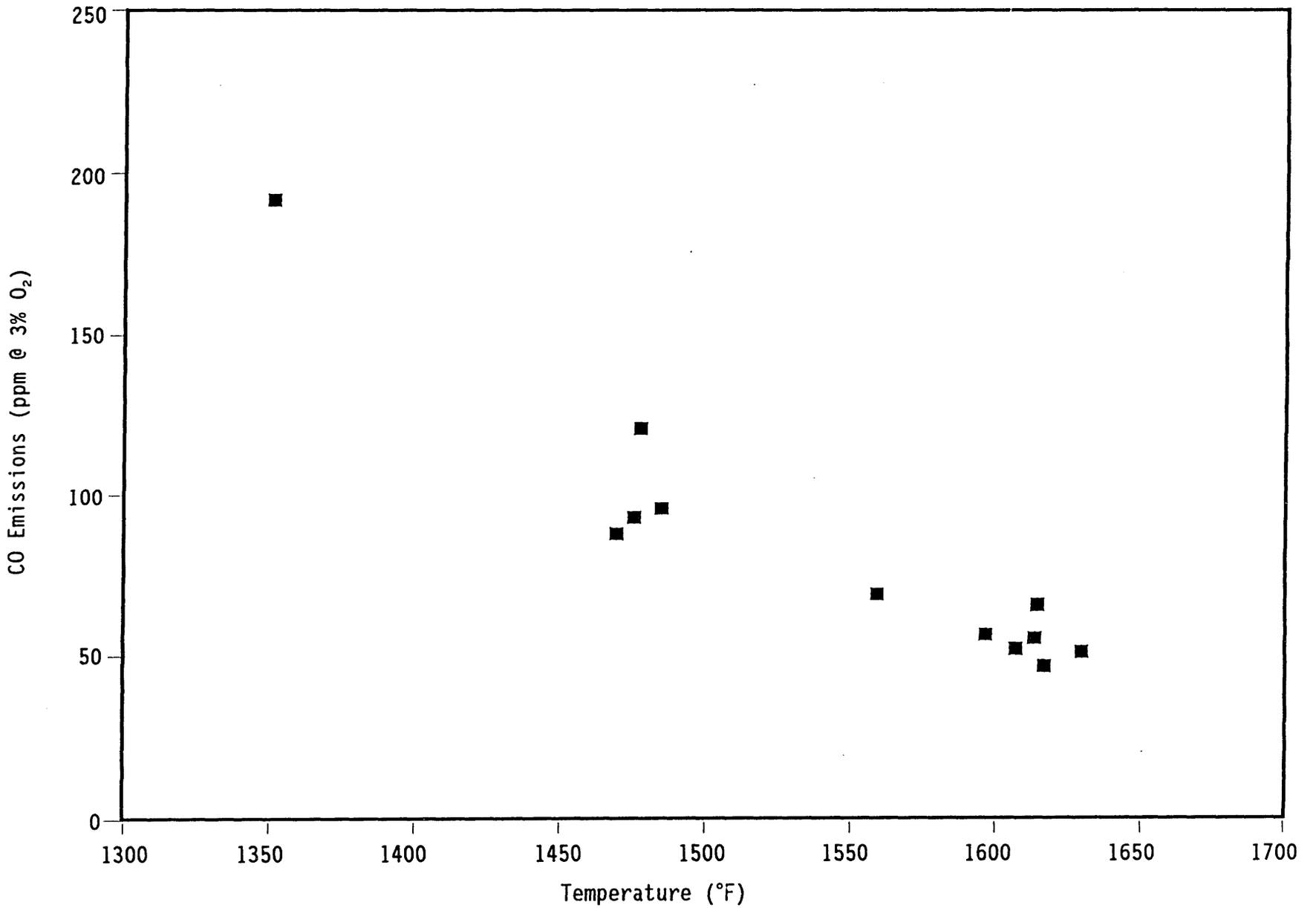

Figure 22. CO emissions as a function of temperature.

8.2 Bed Temperature

The average bed temperature of the EERC combustor at full load is similar to the full-load temperatures at both Nucla and Pyropower. Combustor temperature distributions were also similar between the two pilot units as shown in Figure 23. Partial load in all cases was achieved by reducing the coal feed rate to a percentage of the full-load rate, while maintaining the full-load heat-transfer surface configuration in the combustor. At partial-load conditions, the EERC combustor operated at lower average combustor temperature than either Nucla or Pyropower (Figure 24). The difference is due to the use of an external heat exchanger in the EERC pilot plant. During the 55% load test, the heat-transfer coefficient in the combustor dropped from 21.0 to 14.4 Btu/hr-ft^2-°F, while that in the external heat exchanger only dropped from 105.8 to 96.5 Btu/hr-ft^2-°F, even though two of the three cooling coils used in the full load test were taken off-line in the partial-load tests.

8.3 Sorbent Performance

Some of the factors affecting sulfur capture in a fluidized-bed combustor are temperature, reactivity and particle size of the sorbent, adequate mixing of coal and sorbent, and residence time. In this comparison between the full-scale Nucla station, the Pyropower pilot plant, and the EERC pilot plant, the same coal and limestone were used, eliminating coal and sorbent properties as variables. Maximum sulfur capture occurs at a temperature of about 1550°F; the full-load tests performed at these facilities had average combustor temperatures above 1610°F. Since increasing residence time generally provides better sulfur capture, the full-scale plant, with its taller combustion chamber and operating at similar gas velocity, would be expected to achieve greater sulfur capture. However, pilot-scale units typically have better mixing than full scale, suggesting a better sulfur capture. The SO_2 retention as a function of calcium-to-sulfur ratio is shown in Figure 25. Sulfur retention was similar in the EERC tests. Temperature variations both above and below the optimum temperature of 1550°F resulted in reduced sulfur capture.

Figure 26 shows the effect of calcium-to-sulfur ratio on calcium utilization. Once again, the EERC data points are generally lower than those reported by Pyropower and Nucla. This is consistent with the SO_2 retention findings.

8.4 NO_x Emissions

One advantage of fluidized-bed combustion is the fact that its lower operating temperature creates lower NO_x emissions than a pulverized coal process. Figure 27, NO_x emissions as a function of temperature, shows that there is good agreement between the three plants. The NO_x emissions were higher for those EERC tests performed at a high level of excess air, as expected.

8.5 N_2O Emissions

N_2O emissions are inversely proportional to temperature and directly proportional to oxygen content. Figure 28 shows a comparison between the EERC pilot plant data and that obtained at the Nucla station, both at high and low

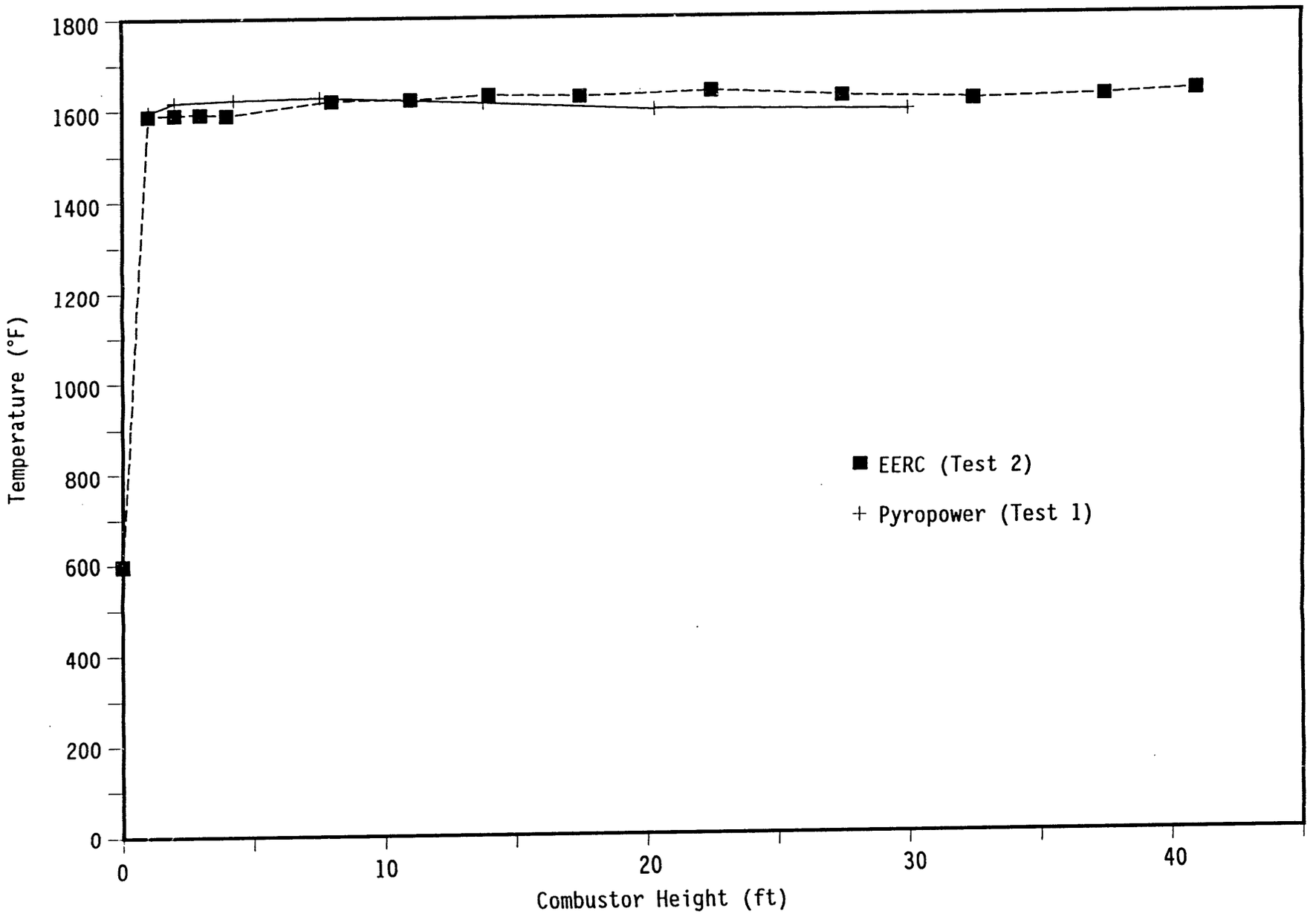

Figure 23. Combustor temperature profiles in the EERC and Pyropower pilot plants.

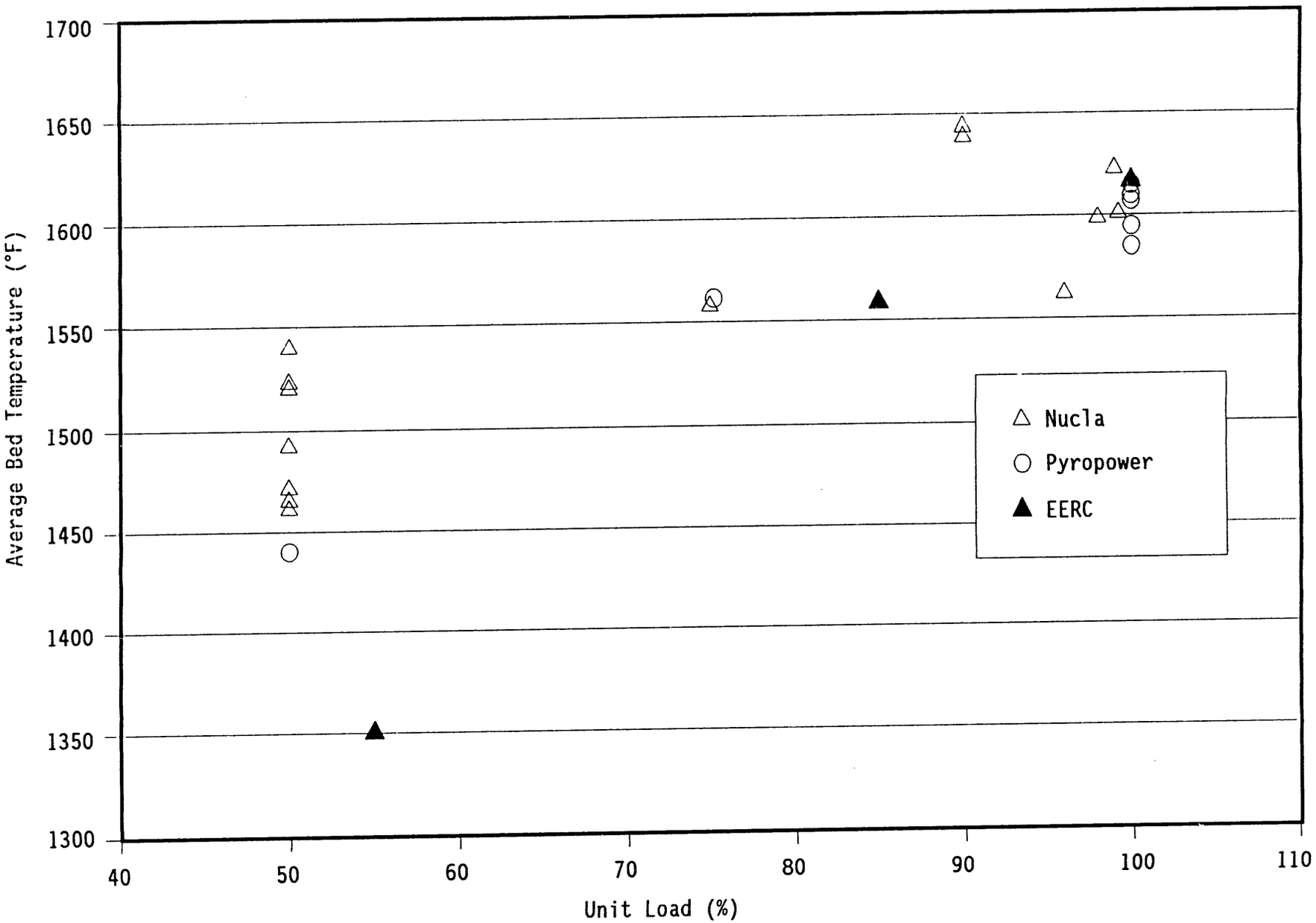

Figure 24. A comparison of bed temperature as a function of load for Nucla, Pyropower, and EERC.

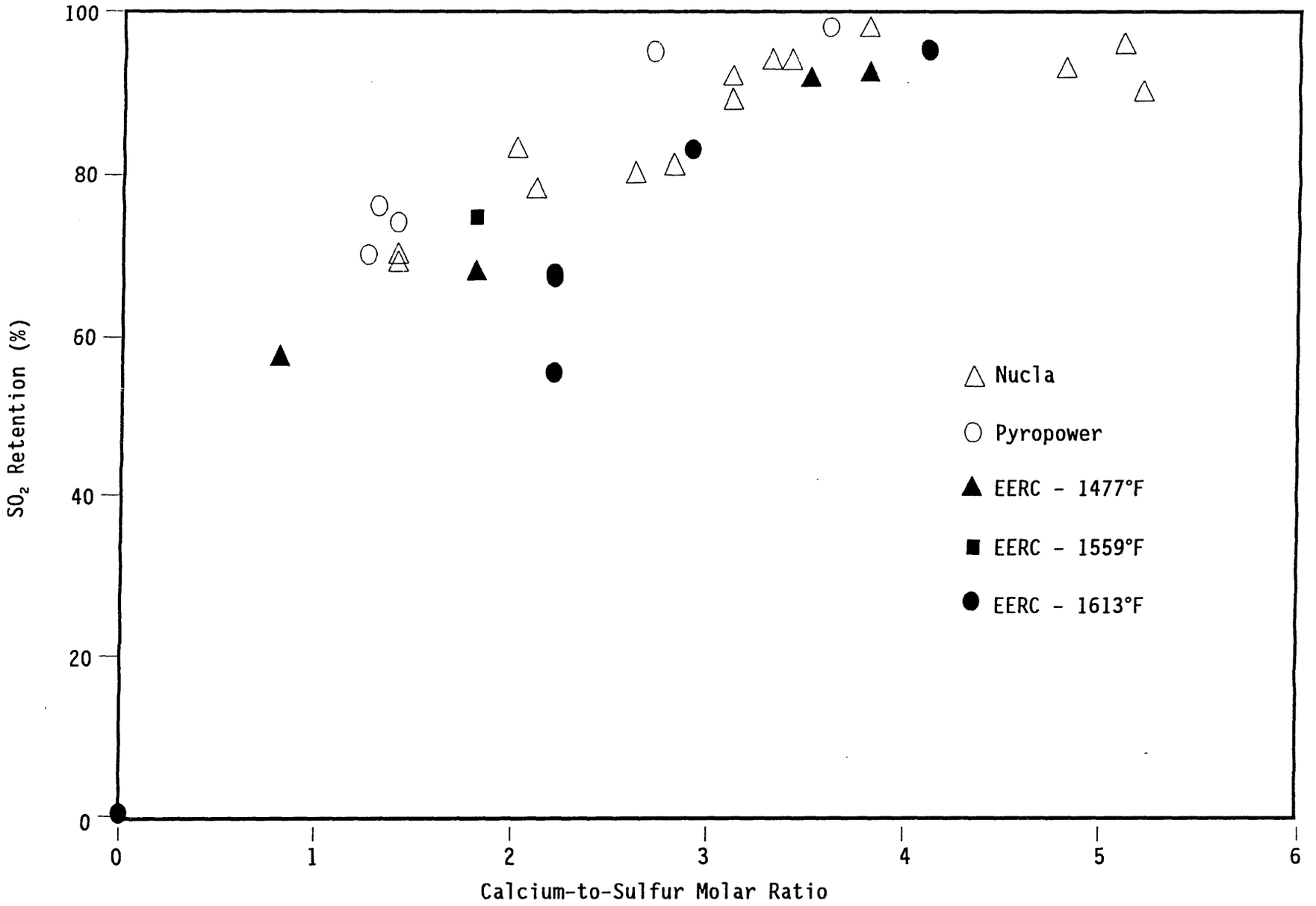

Figure 25. SO_2 retention as a function of calcium-to-sulfur ratio for Nucla, Pyropower, and EERC.

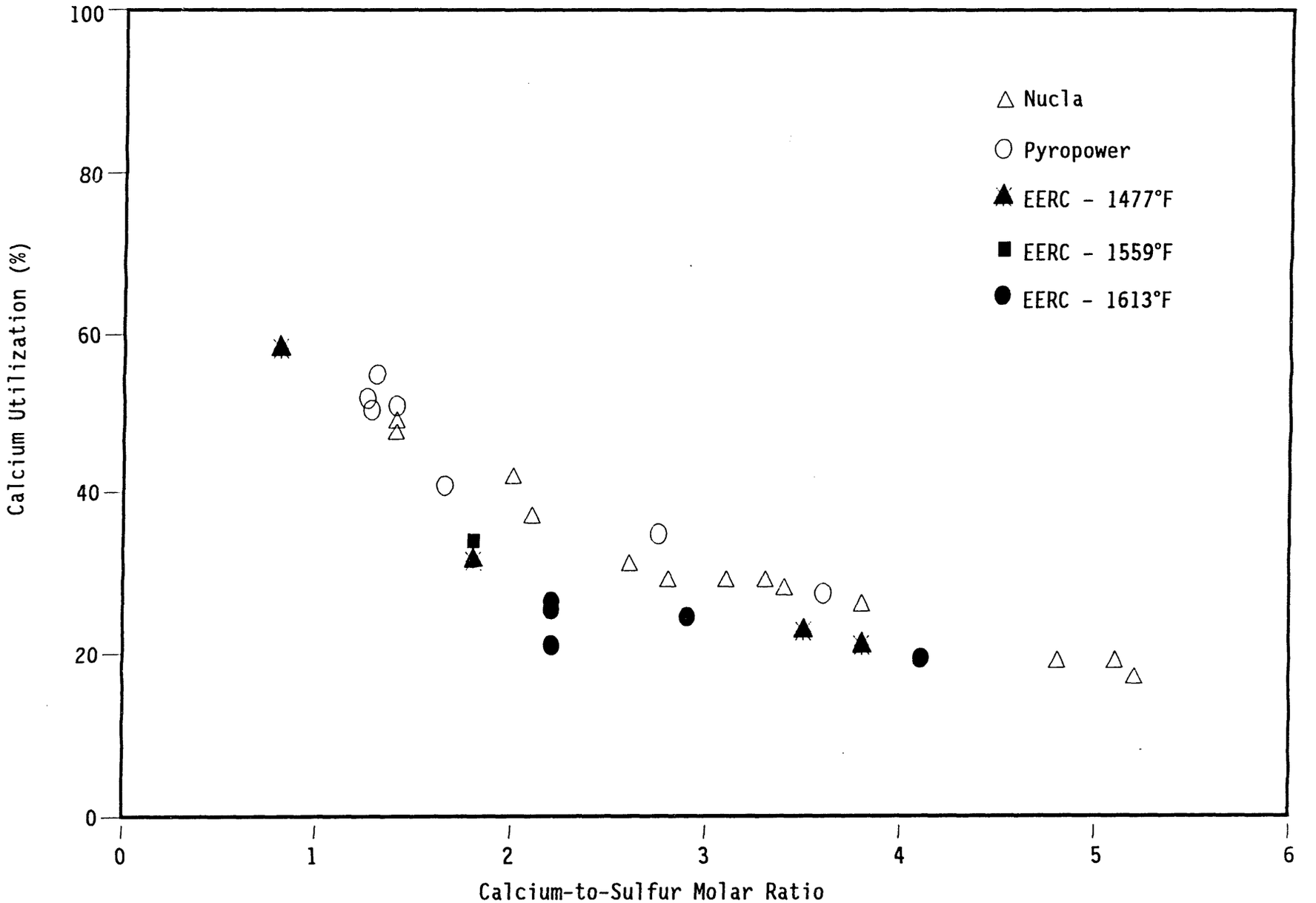

Figure 26. Calcium utilization as a function of calcium-to-sulfur ratio for Nucla, Pyropower, and EERC.

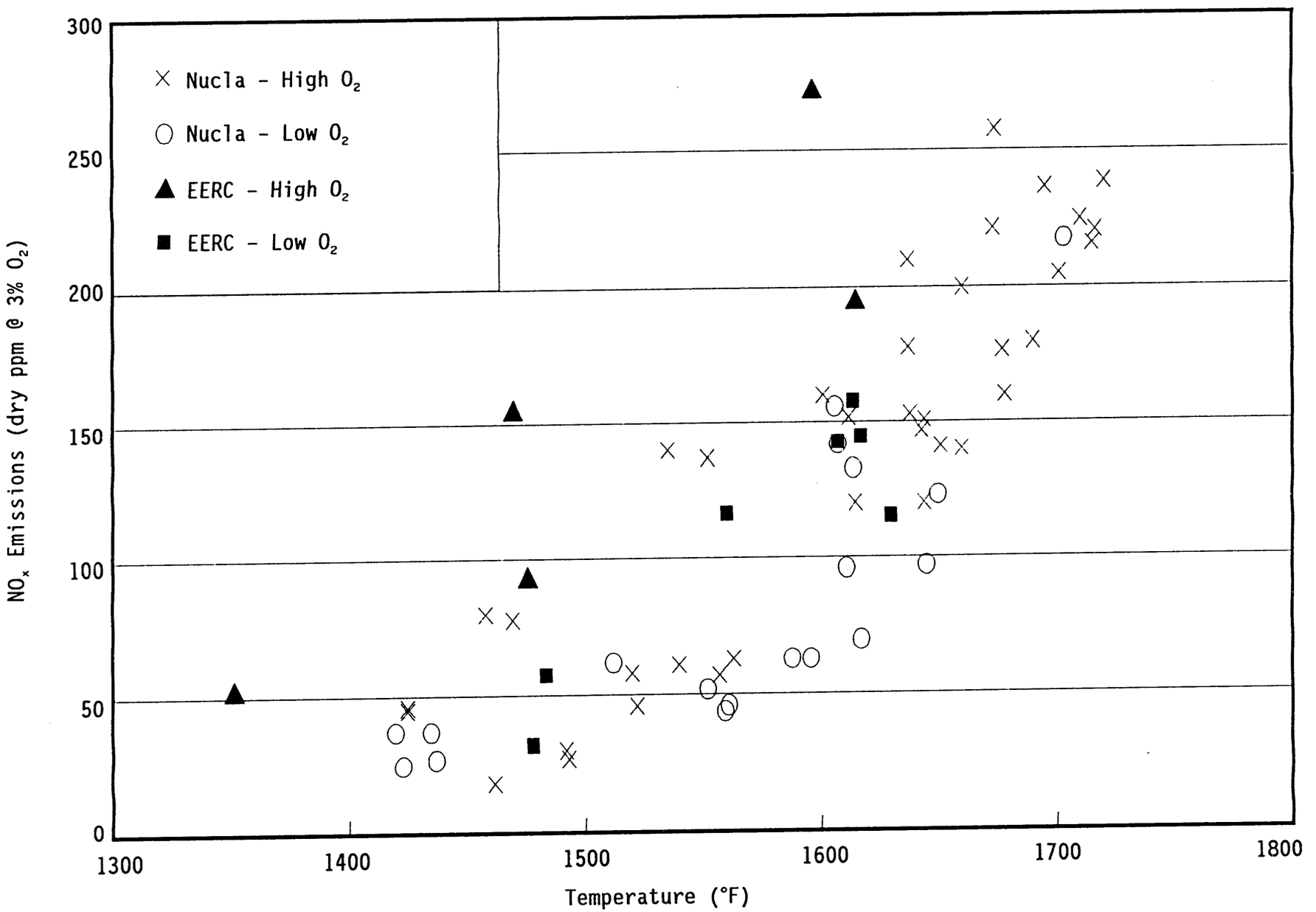

Figure 27. NO_x emissions as a function of temperature for Nucla, Pyropower, and EERC.

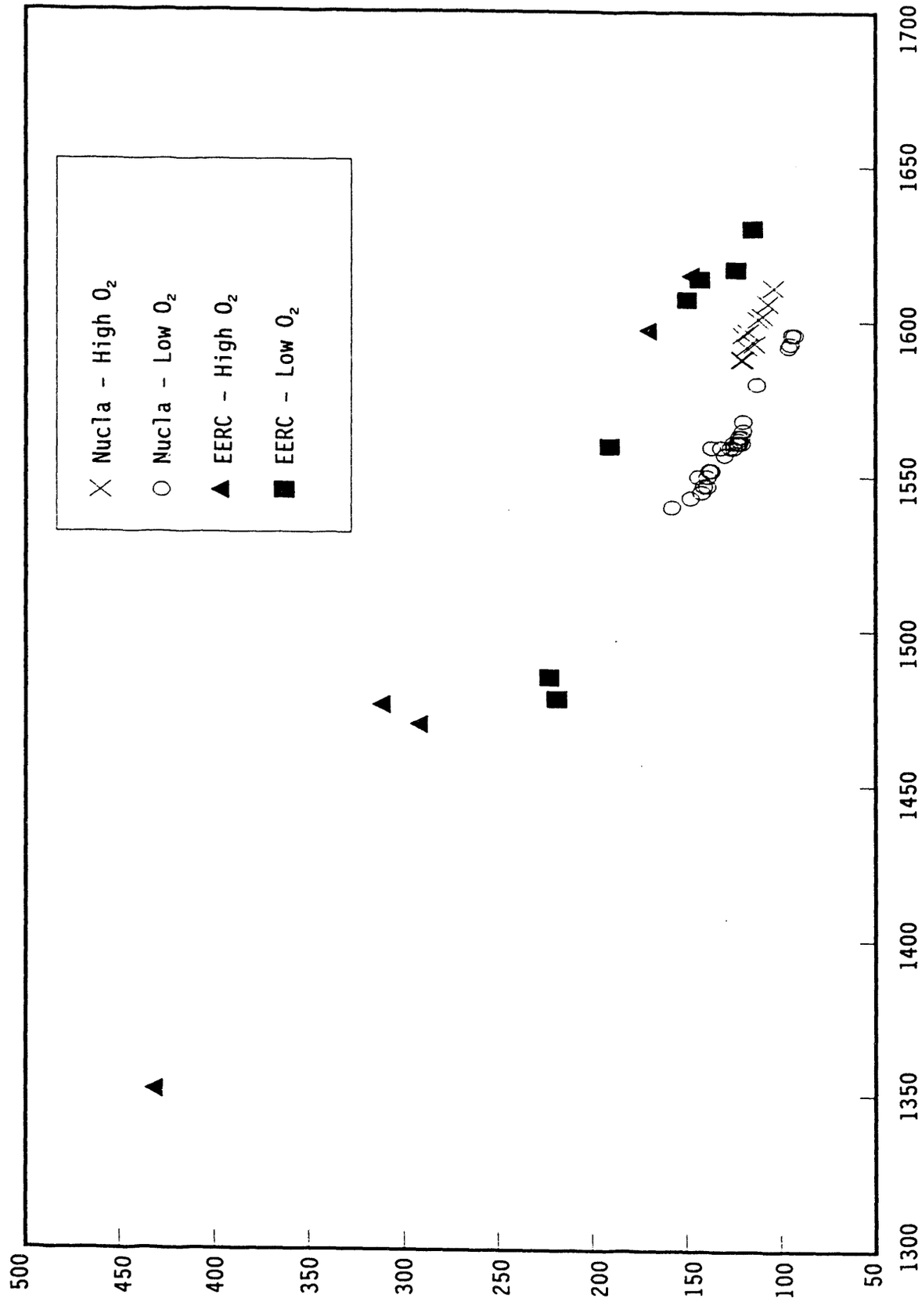

Figure 28. The effects of temperature and oxygen content on N_2O emissions for Nucla and EERC.

oxygen levels. The trends are similar in the two units; the higher N_2O emissions in the pilot plant versus the full-scale plant are consistent with reports from other researchers.

8.6 CO Emissions

The level of carbon monoxide in the flue gas is an indication of combustion efficiency. The levels of CO emissions from the EERC pilot plant are comparable to the Pyropower unit and lower than those from Nucla, as shown in Figure 29. Better mixing at the pilot scale could account for the improvement over Nucla.

8.7 Bottom Ash/Fly Ash Split

The percentage of ash which remains in the combustor or downcomer as bed material compared to that which is carried out of the combustor is a function of the coal and sorbent size, and of the cut point of the cyclone. Figure 30 shows that EERC had a smaller cut point than Nucla and about the same cut point as Pyropower, but the EERC fly ash top size was considerably smaller than either. The bottom ash split for EERC ranged from 28.7% to 79.7% for EERC, while the highest bottom ash split for Nucla and Pyropower were 48% and 22%, respectively. Although cut size may account for some of the difference, the high bottom ash split at EERC may be due in part to a hole in one of the bags and a tendency for the fly ash to hang up in the baghouse hopper, which caused the amount of ash retrieved from the baghouse to be artificially low. This is further evidenced by the poor closure in the ash balance. For comparison to full-scale units, the ash split would need to be adjusted to account for the difference in cyclone cut size.

8.8 Heat Split

The percent of heat removed in the bed (combustor and external heat exchanger) as opposed to the heat removed in the flue gas is more a function of coal type and operating conditions than of test unit. The percent of heat removed in the flue gas was about 40% for both the EERC and Pyropower units. Pyropower had a higher percentage of wall losses - about 19% compared to 11% for the EERC. Heat removal through cooling coils accounted for about 40% of total heat removal in both pilot plants; however, EERC has heat-transfer surfaces in both the combustor and external heat exchanger, while Pyropower only removes heat from the combustor. No data was available from the full-scale unit.

8.9 Combustion Efficiency

Combustion efficiency is a function of temperature, excess air, particle size, and residence time, the last two depending on the design of the combustor. Typically, full scale units have greater residence time, leading to better carbon burnout, but this is offset at the pilot scale by better cyclone efficiency.

The EERC combustion efficiencies shown in Figure 31 are for Tests 5 through 12, both high and low excess air tests. While the low excess air tests are comparable to the Pyropower data, the EERC pilot plant may have slightly higher combustion efficiencies due to greater residence time, since the EERC combustor is 12 feet taller than that at Pyropower. Combustion

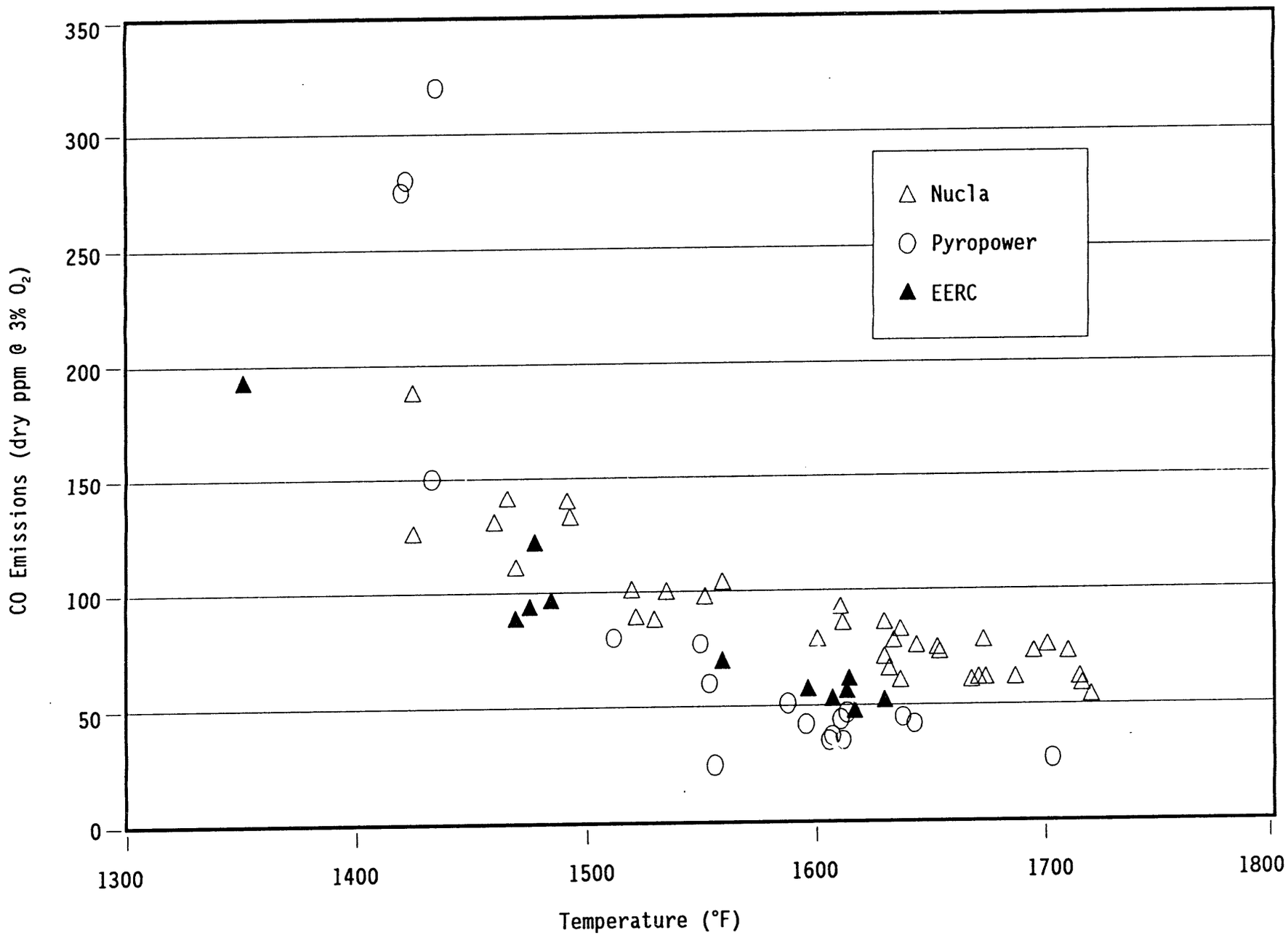

Figure 29. CO emissions as a function of temperature for Nucla, Pyropower, and EERC.

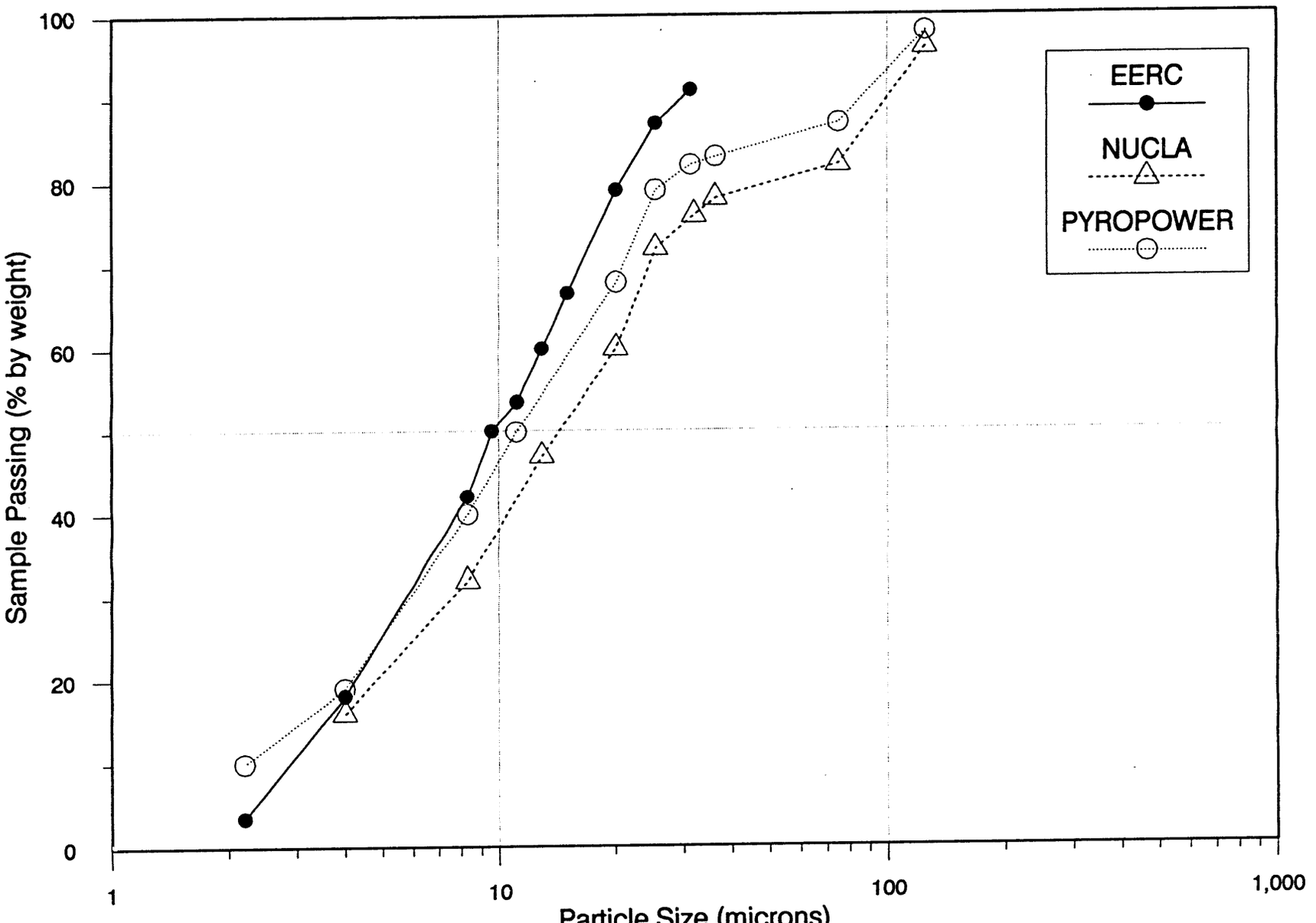

Figure 30. Fly ash size distributions for Nucla, Pyropower, and EERC.

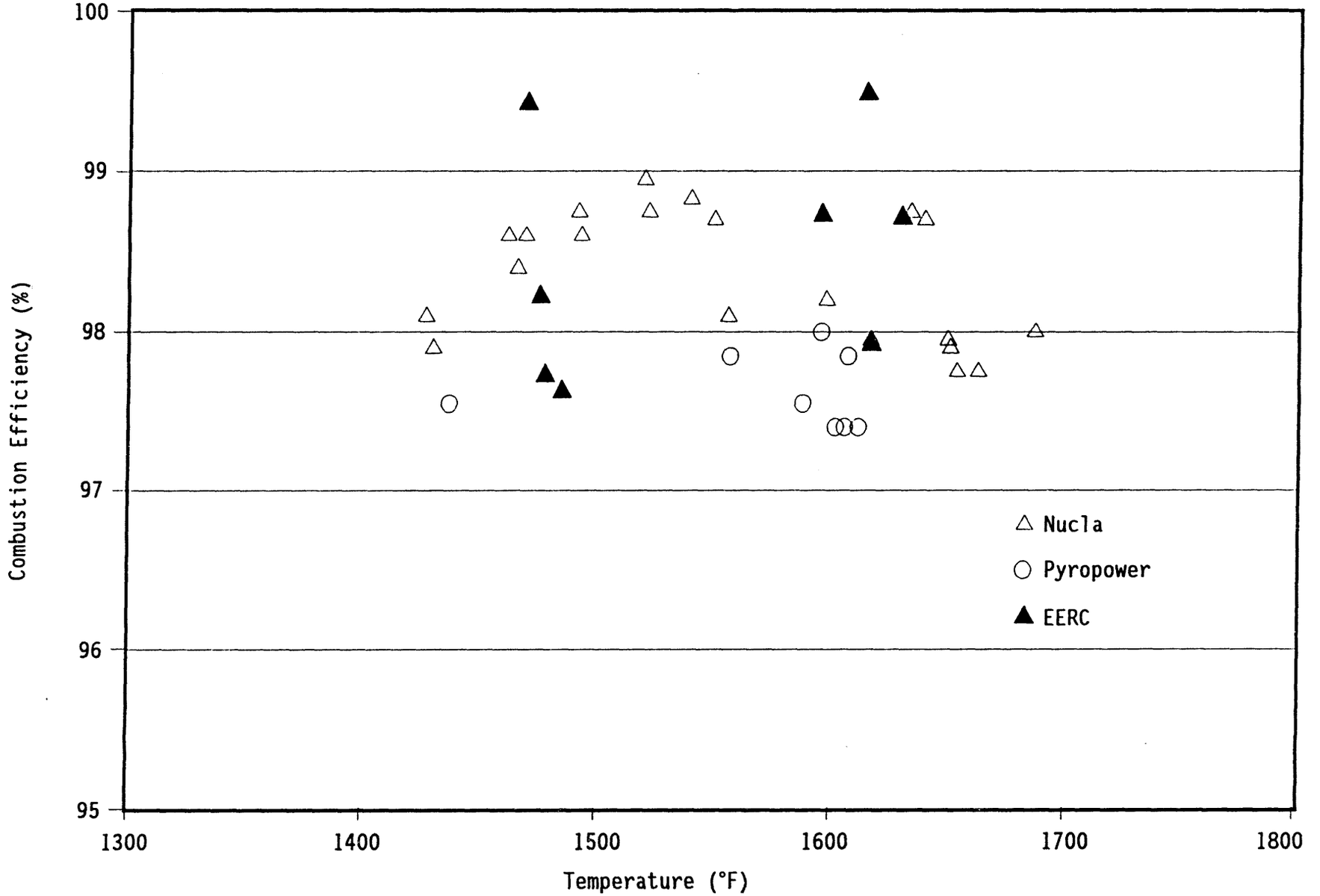

Figure 31. Combustion efficiency as a function of temperature for Nucla, Pyropower, and EERC.

efficiencies from the EERC pilot unit are comparable to those from the Colorado Ute Nucla Station.

9.0 SUMMARY

- In the present configuration, adequate recirculation rates representative of full-scale systems can be obtained, and a high overall bed material particulate capture efficiency of approximately 99.5% was obtained in the particulate collection device.

- Operation of the system at typical full-scale conditions provides scalable heat flux and emissions data. Average heat flux in the combustor was from 24,500 to 35,850 Btu/hr-ft^2 at full-load conditions and 18,030 Btu/hr-ft^2 at 50% load, which is comparable to a full-size system.

- Heat-transfer coefficients decreased in the combustor with increasing height within the combustor from an average of 30.6 Btu/hr-ft^2-°F for Section 2 heat exchangers down to 18.7 Btu/hr-ft^2-°F for Section 8 combustor heat exchangers.

- Bed temperature distribution in the combustor for all full load tests was uniform over the entire height of the combustor.

- Sulfur capture was highest at 1559°F, and an added alkali-to-sulfur ratio greater than 2.5 was required to achieve 70% sulfur retention. Calcium utilization decreased with increasing calcium-to-sulfur molar ratio. No attempt was made during this run to determine the optimal temperature for sulfur control.

- NO_x emissions were in the range of 25 to 280 ppm. NO_x increased with an increase in temperature and/or an increase in excess air, and increased slightly with an increase in calcium-to-sulfur ratio.

- N_2O were greatest at low temperatures. The effect of excess air on N_2O emissions is negligible at high temperatures (greater than 1500°F); however, at lower temperatures, N_2O emissions increased at increased levels of excess air.

- CO emissions were low, ranging from 45 to 145 ppm. The lowest CO emissions occurred at low temperatures.

- Combustion efficiencies ranged from 97.6% to 99.4%. The combustion efficiency increased with increasing bed temperature, excess air, and residence time. The measured combustion effiencies were comparable to those from the Pyropower pilot plant and the Colorado Ute Nucla Station.

- The EERC pilot-scale unit can be used to generate data that is scalable to a full-scale utility plant.

- Tables 18, 19 and 20 summarize factors affecting scalability of CFB data. Both physical parameters and operating conditions have an

effect on unit performance. The tables indicate which parameters can be reliably scaled up, which need to be matched closely to full scale, and which require further research before scalability can be adequately assessed.

TABLE 18

Importance of Physical Configuration on Scalability of CFB Data

Physical Parameters	Effect on Performance	Scalability	Suggestions/Importance
Furnace cross section	Solids/gaseous mixing, emissions, temperature profile, heat absorption pattern.	Smaller cross section of pilot plant allows better mixing of primary and secondary air with fuel, limestone, and recycle. High surface area-to-volume ratio can impact heat removal, if not accounted for in design. Shorter height (residence time) offsets mixing differences to give good combustion efficiency and sorbent performance data. Heat-transfer data can be obtained with properly designed heat-transfer surfaces. The good mixing, especially for secondary air, would tend to lower NO_x emissions; however, the wall effects increase NO_x emissions - the net result is usually higher NO_x emissions from pilot plants. N_2O emissions are also higher in pilot plant.	Refer to Table 18 to determine which parameters are scalable. In designing a new unit, surface-to-volume ratios need to be carefully evaluated. For the EERC unit, heat exchange panels have been designed to allow adequate heat removal while maintaining good temperature distribution.
Particle collection device (cyclone)	Carbon burnout, alkali utilization, ash splits, size of solids in combustion.	Particle collection device that produces the same cut point will give good bed versus fly ash split. A too small cut point will increase carbon burnout and improve alkali utilization. Some argue that the smaller cut point is needed to offset the short residence time, while others contend the cut size should be duplicated to ensure proper ash balances and not to skew performance data to unrealistic high carbon burnout and alkali utilization. Most pilot units with cyclones have a smaller cut point than full-scale units.	If possible, the cut point of the full-scale unit should be matched. This will ensure proper solids distribution in combustor. Good mixing in pilot plant should offset lower residence time. Testing at more than one cut point can demonstrate importance of meeting design cut point in commercial unit.

(continued)

TABLE 18 (continued)

Importance of Physical Configuration on Scalability of CFB Data

Physical Parameters	Effect on Performances	Scalability	Suggestion/Importance
Furnace height/gas residence time	Sulfur capture, CO emissions, combustion efficiency, hydrocarbons.	Shorter residence time, i.e., shorter height, would cause poorer sulfur capture, higher CO and hydrocarbon emissions, and lower combustion efficiency. The superior mixing in the pilot scale versus full scale lessens or, in some cases, totally offsets the lower residence time. Better collection efficiency in cyclone would also improve sulfur capture and combustion efficiency in pilot plant, offsetting residence time effects.	Gas residence time in pilot plant can be matched to full scale by varying velocity. Changes in velocity, however, will impact other conditions such as particle distribution, solids recirculation rate, and bottom-to-total-ash split. It is therefore recommended to operate at same velocity as full scale.
Particle residence time	Sulfur capture, limestone utilization, carbon burnout.	Particle residence time is controlled by combustor height, velocity, wall effects, and cyclone collection efficiency. Longer residence times favor good limestone utilization, sulfur capture, and carbon burnout. The collection efficiency of the cyclone dominates the particle size. Therefore, pilot-scale units with high collection efficiencies may see better performance than full scale. Other factors, such as gas residence time, favor the full-scale plant.	If possible, the cut point (cyclone collection efficiency) in the pilot plant should match the full-scale unit. This would not provide a perfect match between full and pilot scale because of height differences and stronger wall effects of pilot scale.
Hydrodynamics	Additional work needs to be performed to quantify.	Function of size of bed material, recirculation rate, velocity, unit cross section and height, presence of any heat-transfer surfaces in the combustor proper, and amount and location of secondary air.	A number of variables may impact the hydrodynamics of the combustor. More work is needed to assess the magnitude and direction these changes have on scalability.

TABLE 19

Scalability of Operational Parameters from Pilot-Scale CFBC

OPERATIONAL PARAMETERS	EFFECT ON PERFORMANCE	SCALABILITY	SUGGESTIONS/IMPORTANCE
Primary/secondary air split	NO_x emissions, temperature distribution, dense bed height.	Pilot plant is very sensitive to changes in PA/SA. In real life, changes are less pronounced due to poor mixing.	Determine PA/SA ratio that gives lowest NO_x without greatly impacting temperature profile. Run all tests at optimum PA/SA. Compare relative differences in NO_x between tests.
Bed temperature	Carbon burnout, optimum sorbent utilization, NO_x and CO emissions, heat absorption pattern.	Temperature effects appear to scale well between pilot and commercial units. These performances are also impacted by residence times.	Test at various temperatures within the range of characteristics of full-scale units.
Load	Heat absorption patterns, CO and NO_x emissions, carbon burnout, thermal efficiency, temperature distribution.	Data will be somewhat scalable if the correct temperature profiles are maintained. Mixing patterns may differ between units at low velocity, high excess air. Good mixing in pilot plant should offset lower residence time.	It is important to match the temperature distribution of the commercial unit. Impacts of velocity and excess air changes should be evaluated. Load-following methods of Pyropower should be compared to CE/Lurgi.
Excess air	Thermal efficiency, CO and NO_x emissions, carbon burnout.	At very low excess air levels, pilot scale may give better performance due to good air/solids mixing and distribution. Trends should be similar at high excess air levels.	Test at low and high excess air levels. Keep in mind that at normal operation, excess air will not vary significantly. Only during load following and upset conditions will large variations be seen.
Calcium-to-sulfur ratio	Sulfur capture, limestone utilization, waste/disposal volumes, particulate generation.	Scalability generally quite good. Most SO_2 released in bottom of bed height. Good mixing in pilot also decreases importance of height.	Determine Ca/S to meet NSPS. Tests at varying Ca/S can be performed to determine Ca/S to achieve other conditions. Bottom ash/fly ash split is important.
Solids recirculation rate	Control load, heat absorption pattern, heat-transfer coefficient.	Heat transfer shows good scalability.	Operate at representative recirculation rate approximately of 15-20 kg/m^2-sec.
Fuel size	Carbon burnout, bed versus fly ash split, solids density in combustor.	Bed versus fly ash split scalable, providing particle collection device operates at the same cut point. Carbon burnout similar. (Good mixing offsets short height in pilot plant.)	It is important to match the fuel spec of the vendor or duplicate that in an operating unit.
Limestone size	Required Ca/S, bed versus fly ash split.	Good scalability if particle collection operates at same cut point.	Duplicate design size for unit (expected delivered size from quarry/supplier).

TABLE 20

Scalability of Measured Performance Parameters from Pilot-Scale CFBC

Performance Parameter	Scalability
Heat transfer	Heat transfer is primarily a function of the recirculation rate and the particle-size distribution in the combustor. Good correlation between the pilot- and full-scale units can be expected if these two parameters can be controlled, as seen by the EERC data.
Combustion efficiency	Carbon burnout will be controlled mainly by the cut point of the cyclone, with better carbon burnout being achieved for smaller cut points. CO will decrease as the gas residence, or combustor height, decreases, but should increase for well-mixed systems. Therefore, carbon burnout should be similar between full- and pilot-scale units if the cut point is similar. The impact of combustor height versus gas mixing offset each other from full- to pilot-scale systems, making overall combustion efficiency a scalable parameter.
Bottom ash/total ash split	The percentage of bottom ash will be primarily determined by size of the coal ash and limestone, and by the cut size of the cyclone. Assuming the same coal and limestone sizing is used for the pilot- and full-scale testing, similar ash splits will be obtained only if the cyclone cut size is the same. If a smaller cut size is obtained in the pilot scale, as was done at EERC versus the Colorado Ute Nucla Station, a higher fraction of the ash will be bottom ash.
Bed grain size	Assuming the same coal and limestone sizes are used for both systems, the bed grain size will be primarily a function of the cut size of the cyclone. However, unless there is a large difference in cut size between the full- and pilot-scale units, the bed grain size will be approximately the same.
Limestone utilization,sulfur capture,Ca/S ratio	Sulfur capture and limestone utilization between the full- and pilot-scale units are similar. Shorter combustor heights in pilot plants are offset by better particle and gas mixing. Smaller cyclone cut points in many pilot plants also favor better performance. Data from the EERC and the Pyropower pilot plant indicate similar performance to the Colorado Nucla Station. The scalability of this data may change with differing full-scale designs.
CO emissions	CO emissions would be expected to increase in pilot plants because of the shorter residence times, but decrease because of the improved gas mixing. The net effect for the EERC pilot plant is a decrease in CO emissions as compared to full scale.
NO_x, N_2O emissions	NO_x emissions in the pilot plant are often higher than in full-scale units because of the high surface-to-volume ratio of the pilot plant. Better gas mixing in the pilot scale, especially of the secondary air, however, tends to reduce the NO_x in the pilot scale. NO_x emissions from the EERC pilot

(continued)

TABLE 20 (continued)

Scalability of Measured Performance Parameters from Pilot-Scale CFBC

N_2O, N_2O emissions (continued)	plant and Colorado Ute Nucla Station were similar. N_2O emissions have been observed by a number of researchers to be higher in pilot plants than for full-scale units, probably due to gas residence time effects, although wall effects may also be important. Data generated by EERC showed similar trends of N_2O emissions with respect to operating conditions, but were consistently higher than those from the full-scale unit.

DOE/MC/26050-3037

Validation Testing of the EERC Pilot-Scale Circulating Fluidized-Bed Combustor Using Salt Creek Coal

DOE

END

DATE FILMED

2/27/92